Acta Crystallographica Section B
Structural Science
ISSN 0108-7681

5*d* and 4*f* electron configuration of CeB_6 at 340 and 535 K

Ryoko Makita,[a]* Kiyoaki Tanaka[a] and Yoshichika Ōnuki[b]

[a]Graduate School of Materials Science and Engineering, Nagoya Institute of Technology, Japan, and [b]Graduate School of Science, Osaka University, Japan

Correspondence e-mail: 14515020@stn.nitech.ac.jp

Received 17 April 2008
Accepted 18 August 2008

X-ray atomic orbital (XAO) analysis revealed that at both temperatures the electrons are transferred from B $2p_x(=p_y)$ to Ce 5*d* and 4*f* orbitals. At 340 K $5d(j = 5/2)\Gamma_8$ orbitals are occupied partially, but $4f(j = 5/2)\Gamma_8$ orbitals are more populated than $4f(j = 5/2)\Gamma_7$ orbitals, in contrast to our observation at 430 K [Makita *et al.* (2007). *Acta Cryst.* B**63**, 683–692]. At 535 K the XAO analysis revealed clearly that the order of the energy levels of $4f(j = 5/2)\Gamma_8$ and Γ_7 states reversed again and is the same as that at room temperature. It also limited the possible 5*d* configurations to three models among the nine possible ones. However, the XAO analysis could not decide which of the three models was the best with the present accuracy of the measurement. Two of them have partially and fully occupied $5d(j = 5/2)\Gamma_7$ orbitals and the remaining one has a fully occupied $5d(j = 3/2)\Gamma_8$ orbital. Since the lobes of $5d(j = 3/2)\Gamma_8$ or $5d(j = 5/2)\Gamma_7$ orbitals do not overlap with the $4f(j = 5/2)\Gamma_8$ orbitals as well as the $5d(j = 5/2)\Gamma_8$ orbitals, the order of the energy levels of the $4f(j = 5/2)$ orbitals became the same as that at room temperature. These results indicate that the crystal field varies with temperature due to the electron transfer from B 2*p* to Ce 5*d* orbitals. The difference densities after the spherical-atom refinement at the three temperatures clearly revealed the different combinations of 4*f* and 5*d* orbitals which are occupied. In the present study positive peaks due to the 4*f* electrons appear near the Ce nucleus and those due to 5*d* orbitals are found in the area outside the 4*f* peaks. Between the two areas there is a negative area distributed spherically at 340 K. The negative area produced by the contraction of $4f(j = 5/2)\Gamma_8$ orbitals seems to reduce the electron repulsion of the $5d(j = 5/2)\Gamma_8$ orbitals and helps the $4f(j = 5/2)\Gamma_8$ orbitals to remain as the ground state.

1. Introduction

CeB_6 has been investigated intensively at low temperature due to its many interesting properties such as antiferro-quadrupolar (AFQ) ordering and competition for the Kondo effect, which makes the localized spin of Ce vanish owing to the coupling of Ce and B spins, and the Ruderman–Küttel–Kasuya–Yoshida (RKKY) interaction, which arranges the spin of the antiferromagnetic interaction of Ce with the spins of itinerant electrons of B (Sato *et al.*, 1985; Sakai *et al.*, 1997). These properties are closely connected with the localized $4f$-Γ_8 electrons of Ce and conductive electrons of B.

In our previous study (Makita *et al.*, 2007; hereinafter referred to as MTOT) the electron-density distribution (EDD) in CeB_6 was measured at 430 K and analyzed with the XAO analysis method (Tanaka *et al.*, 2008) and several interesting facts were found. At high temperature electrons

were transferred from B $2p_x(=p_y)$ to the Ce $5d(j = 5/2)\Gamma_8$ orbitals, and the $4f$-Γ_7 state, which is above $4f$-Γ_8 in energy at 298 K, was more populated than the $4f$-Γ_8 orbitals. Electron transfer from the B_6 moiety to Ce $5d$ orbitals is a reversal of that found at low temperatures (Tanaka & Ōnuki, 2002). Since the filled $5d(j = 5/2)\Gamma_8$ orbitals are outside the $4f$ orbitals and both $5d(j = 5/2)\Gamma_8$ and $4f(j = 5/2)\Gamma_8$ orbitals have the same Γ_8 symmetry, with the EDD extending to the same directions, the $4f(j = 5/2)\Gamma_8$ orbitals became unstable, thus making the $4f$-Γ_7 orbital more populated than the $4f$-Γ_8 orbitals. In order to assess and integrate these results the electron-density distribution (EDD) was measured at 340 and 535 K with a four-circle diffractometer equipped with a small furnace. Furthermore, the fully occupied $5d$ orbitals imply that energy can be gained from the $5d \rightarrow 4f$ transition at temperatures below 473 K. The energy gap between $4f$ and $5d$ in $[Ce(OH_2)_9]^{3+}$ was measured by UV absorption spectroscopy (Okada *et al.*, 1985) to be 30–32 $\times 10^3$ cm^{-1} or 3.7–4.0 eV. The $4f \rightarrow 5d$ energy gap in CeB_6 is expected to be similar. Therefore, it becomes highly interesting whether the $5d$ occupation occurs below 474 K or not. The measurement at 535 K was planned since it is close to the energy difference between the $4f$-Γ_8 and Γ_7 states in CeB_6.

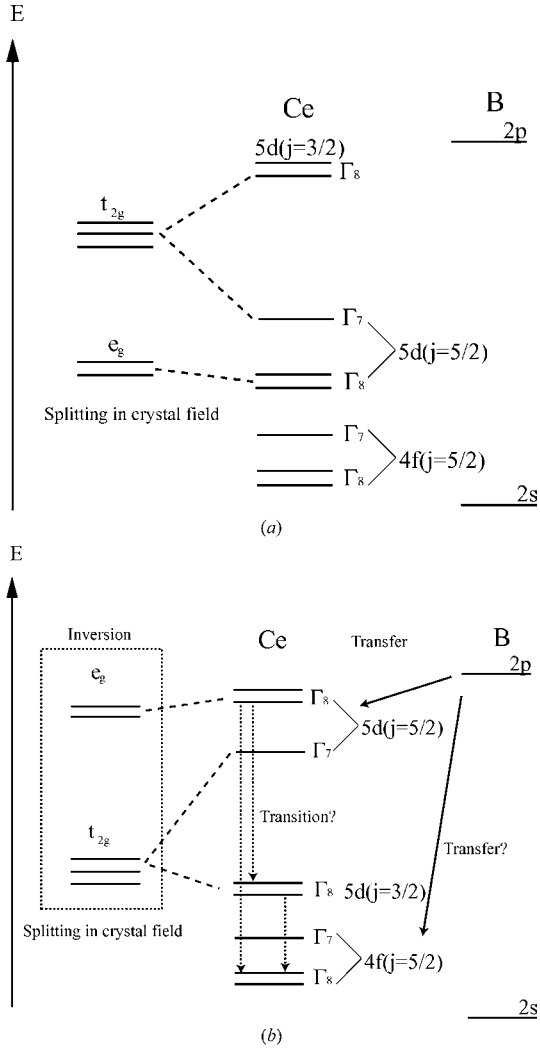

Figure 1
Schematic drawing of the energy levels of Ce and B (*a*) below room temperature and (*b*) at 535 K. The energy levels of Ce were estimated using the program *HEX* (Liberman *et al.*, 1971), those of B were calculated by Mann (1968). The energy difference between $5d$ and $4f$ levels is approximately 56 times larger than that between $4f$-Γ_8 and Γ_7 orbitals.

Several investigations have been reported on the important contributions of the $5d$ electrons to physical properties. Resonant X-ray scattering intensities corresponding to the AFQ superlattice spot are explained by the mechanism that $5d$ electrons excited from B $2p$ modulate through the Coulomb interaction between $4f$ and $5d$ electrons (Nagao & Igarashi, 2002). On the other hand, Ignatov *et al.* (2006) related the anomalous behaviour of the transport characteristics at ~ 80 K to the instability of the exciton in the $5d$ band. The EDD of CeB_6 at 298 K, from synchrotron X-ray diffraction reported by Streltsov *et al.* (1999), showed positive peaks at ~ 1.5–2 Å from the Ce site. They regarded these peaks as mixing the $4f$ wavefunction with $5d$ or $2p$ components. Grushko *et al.* (1985) compared the X-ray chemical shift with the self-consistent Dirac–Fock–Slater–Latter calculation and concluded that the trivalent rare-earth atoms in hexaboride with metallic conduction donate two electrons to the boron framework, and that a third valence electron exists in the $5d$ orbitals. From the band structure of CeB_6, the $4f$ bands are hybridized with the $5d$ band around the Fermi energy (Heide *et al.*, 1986) and the Fermi surface of CeB_6, centred at the X point in the Brillouin Zone which is the centre of the B—B bond between the B_6 octahedra (hereinafter referred to as $B—B_{out}$), has the hybridized character of the Ce $5d$ and B $2p$ states (Souma *et al.*, 2004). Thus, it is worth including the $5d$ orbitals in the XAO analysis at high temperature.

Ce^{3+} formally has one $4f$ electron. When the spin-orbit interaction is taken into account, the $4f$ orbitals split into two $4f$ states with $j = 5/2$ and $j = 7/2$. Since the energy of the latter is higher and no electrons are found on them in our studies on CeB_6, only the $4f(j = 5/2)$ orbitals are considered in the present study. In the O_h crystal field the $4f(j = 5/2)$ orbitals split further into two orbitals: Γ_7 (doublet) excited states and Γ_8 (quartet) ground states. The EDDs of the Γ_7 orbitals extend along the $\langle 111\rangle$ and $\langle 110\rangle$ directions, whereas the Γ_8 orbitals extend along the $\langle 100\rangle$ direction. The excitation energy between Γ_7 and Γ_8 was reported to be 530–560 K (Loewenhaupt *et al.*, 1985; Zirngiebl *et al.*, 1984). In the present study, the temperature T was used as the expression of energy rather than k_BT (k_B is Boltzmann's constant). The energy levels of the $5d$ orbitals of CeB_6 split into $5d(j = 3/2)$, $5d(j = 5/2)\Gamma_8$ and $5d(j = 5/2)\Gamma_7$ orbitals owing to the crystal field and spin-orbit interaction. The $5d(j = 3/2)$ orbitals have fourfold degeneracy, with Γ_8 symmetry. The $5d(j = 5/2)\Gamma_7$ and Γ_8 orbitals have lobes extending to the same directions as the $4f(j = 5/2)\Gamma_7$ and Γ_8 orbitals.

The schematic energy levels are illustrated in Fig. 1(*a*) for the forthcoming discussion. The energy levels of Ce $4f(j = 5/2)$, $5d(j = 5/2)$ and $5d(j = 3/2)$ are calculated using the program *HEX* (Liberman *et al.*, 1971) assuming a $4f(j = 5/2)^1 5d(j = 5/2)^{0.5} 5d(j = 3/2)^{0.5}$ configuration. They are −0.74, −0.63 and

Table 1
Experimental details.

	340 K	535 K
Crystal data		
Chemical formula	$B_6^{3-}Ce^{3+}$	$B_6^{3-}Ce^{3+}$
M_r	204.98	204.98
Cell setting, space group	Cubic, $Pm\bar{3}m$	Cubic, $Pm\bar{3}m$
Temperature (K)	338.4 (9)	535 (2)
a (Å)	4.14288 (3)	4.14918 (4)
V (Å^3)	71.11 (1)	71.43 (1)
Z	1	1
D_x (Mg m−3)	4.787	4.765
Radiation type	Mo $K\alpha$	Mo $K\alpha$
μ (mm^{-1})	15.66	15.59
Crystal form, colour	Sphere, metallic dark purple	Sphere, metallic dark purple
Crystal radius (mm)	0.037	0.037
Data collection		
Diffractometer	Four-circle	Four-circle
Data collection method	Integrated intensities data from $\omega/2\theta$ scans	Integrated intensities data from $\omega/2\theta$ scans
Scan speed in ω (min^{-1})	2	2
Maximum no. of scans	10	10
Absorption correction	For a sphere	For a sphere
T_{min}	0.434	0.435
T_{max}	0.483	0.484
No. of measured, independent and observed reflections	902, 180, 179	1066, 182, 171
Criterion for observed reflections	$F > 3.0\sigma(F)$	$F > 3.0\sigma(F)$
R_{int}	0.006	0.008
θ_{max} (°)	74.3	74.0
No. and frequency of standard reflections	3 every 50 reflections	3 every 50 reflections
Refinement		
Refinement on	F	F
$R[F^2 > 2\sigma(F^2)]$, $wR(F^2)$, S	0.008, 0.010, 1.04	0.009, 0.013, 1.30
No. of reflections	804	809
No. of parameters	38	38
Weighting scheme	Based on measured s.u.s	Based on measured s.u.s
$(\Delta/\sigma)_{max}$	< 0.0001	< 0.0001
$\Delta\rho_{max}$, $\Delta\rho_{min}$ (e Å−3)	0.70, −0.39	0.55, −0.37
Extinction method	B–C type 1 Gaussian anisotropic	B–C type 1 Gaussian anisotropic
Extinction coefficient	0.251 (2) × 10^4	0.290 (2) × 10^4

Computer programs used: *IUANGLE* (Tanaka *et al.*, 1994), *RSLC-3 UNICS* system (Sakurai & Kobayashi, 1979).

−0.64 a.u. for 4*f*(j = 5/2), 5*d*(j = 5/2) and 5*d*(j = 3/2). When the crystal field is taken into account and the quantization axes are taken along the ⟨100⟩ direction, to the face centres of the cubic cell, the energy level of 5*d*(j = 5/2) is expected to be lower than that of 5*d*(j = 3/2) orbitals, since the energy level of 5*d*-e_g extending along the ⟨100⟩ directions is lower than that of the 5*d*-t_{2g} orbitals, which correspond to the 5*d*(j = 3/2) orbitals. On the other hand, those of B 2*s* and 2*p* levels are −0.98 and −0.62 a.u. according to Mann (1968). Many electrons were found in 5*d* orbitals, but no electrons were found in 4*f*(j = 7/2) orbitals in any of the refinements of the present study. Since the 4*f* orbitals are located closer to the nucleus and the effect of the crystal field is shielded by the 5*p* orbitals outside of them, the energy levels of the 4*f* orbitals are dominated by the spin-orbit interaction rather than by the crystal field. Hence, the energy level of the 4*f*(j = 5/2) orbitals remains lower than the 4*f*(j = 7/2) orbitals and no electrons were found in the orbital after the refinement.

2. Experimental

Although the experimental equipment and procedures at 340 and 535 K were almost the same as those described in MTOT, the specimens used in each experiment were not identical. The CeB_6 single crystal was shaped into a sphere with a radius of 37 µm. X-ray intensity was measured using a four-circle diffractometer (MAC Science). The crystal was heated in a furnace installed on the diffractometer. The temperature of the sample depends on the χ angle of the diffractometer and the temperature distribution at the sample position was measured by shifting χ angles of the diffractometer, keeping an electric current in the Pt wire at 2.02 A. When χ was limited between −50 and 80°, the temperature of the crystal was kept at 338.4 ± 0.9 K. The current of 5.0 A kept the temperature of the crystal at 535 ± 2.0 K, limiting the χ angle between −60 and 40°.

Measurements were taken after heating the crystal for 1 h to stabilize the temperature. The orientation matrix and the lattice parameters were determined by {155}, {444}, {172} and {633} reflections with $2\theta \simeq 75°$, where $K\alpha_1$ radiation was well separated from $K\alpha_2$. Since the contribution of 4*f* electrons to structure factors is very small, the fluctuations of the observed structure factors caused by the multiple diffraction, which easily exceed 1%, make accurate measurement of 4*f*-EDD difficult, as demonstrated in Fig. 2 of the paper written by Tanaka & Ōnuki (2002). Proper treatment of this effect is essential for the EDD measurement of rare-earth compounds. Since multiple diffraction is very sensitive to the orientation of the crystal, a subtle change in the X-ray beam path such as that in the orientation of the monochromator may easily change the effect and the correction for it may not be realistic. Tanaka & Ōnuki (2002) succeeded in measuring the 4*f*-EDD of CeB_6 by avoiding the multiple diffraction with a φ scan and they also succeeded in treating the localized electron densities quantitatively using XAO analysis. In the present study the optimum φ angles (keeping the effect less than 0.25% of each structure factor) were calculated using the program *IUANGLE*

(Tanaka *et al.*, 1994). Other data collection details are summarized in Table 1.[1]

2.1. Shielding of the X-rays by the Pt wire of the furnace

In the present study the Pt wire of the furnace was extended around the crystal to stabilize the temperature, but it is accompanied by unavoidable scattering and shielding of the incident and diffracted X-rays by the Pt wire. Therefore, at 340 K 75 reflections were rejected, among which 64 reflections were partially shielded when the difference of 2θ and ω was 60–70°, and 11 reflections with an anomalous background caused by the scattering of the incident beam by the Pt wire. In addition, 23 reflections with $F < 3\sigma F$ were considered to be insignificant. Hence, 98 reflections were rejected. After this process the number of independent reflections was reduced from 180 to 179.

On the other hand, at 535 K 169 reflections were rejected, among which 58 reflections were shielded and 111 reflections had an anomalous background. In addition, 71 reflections with $\sin\theta/\lambda > 1.34$ ($2\theta \geq 145°$) were rejected because of the high background due to the air scattering of the incident X-rays. Five reflections that have more than three equivalent reflections deviate too much from the mean of the equivalent ones for an unknown reason were rejected. 12 reflections with $F < 3\sigma F$ were considered to be insignificant. Hence, 257 reflections were rejected. After this process the number of independent reflections was reduced from 182 to 171. Among 11 independent reflections deleted, 6 reflections have $\sin\theta/\lambda > 1.34$. The remaining 5 reflections were affected by the Pt wire, but $\sin\theta/\lambda \simeq 1.33$. The number of reflections with an anomalous background at 340 K was less than that at 430 and 535 K, which may be caused by a slight change in the setting of the Pt wire. Only $R_{\rm int}$ in Table 1 is calculated, excluding the reflections affected by the Pt wire.

3. Refinement

The reflection data at 340 and 535 K were refined using the least-squares program *QNTAO* (K. T., see also Tanaka & Ōnuki, 2002; Tanaka *et al.*, 2008). The valences of Ce and B were initially assumed to be +3 and −0.5, and electrons were configured equally among the subshell orbitals. The process makes the EDD of each atom spherical. We call this stage the spherical-atom refinement (hereinafter referred to as refinement *A*). A spin-orbit interaction was assumed for Ce and a scattering factor was calculated using the program *SFRSCF* (K. T., see also Tanaka & Ōnuki, 2002) from relativistic atomic orbitals, which were calculated by Tatewaki using the program *GRASP* (Dyall *et al.*, 1989). The scattering factors of B were calculated based on self-consistent field wavefunctions (Mann, 1968). Anomalous dispersion terms of each atom were taken from *International Tables for X-ray Crystallography* (1992, Vol. C). We assumed that extinction is type I (Becker & Coppens, 1974*a*,*b*, 1975) based on the Thornley–Nelmes distribution function (Thornley & Nelmes, 1974). After spherical-atom refinement, an XAO analysis was carried out which included analysis of the anharmonic vibration (AHV) of each atom.

3.1. Anharmonic vibration

Dawson *et al.* (1967) proposed the treatment of temperature factors, including the anharmonic thermal vibration effect for high-symmetry crystals by means of series expansion of a one-particle potential. Tanaka & Marumo (1983) generalized the treatment and anharmonic third- and fourth-order parameters were refined in the least-squares program. AHV parameters were restricted by the site symmetry of Ce($m\bar{3}m$) and B($4mm$), and their potentials, V, are represented by

$$\begin{aligned} V_{\rm Ce} &= b_1(u_1^2+u_2^2+u_3^2) + q_{1111}(u_1^4+u_2^4+u_3^4) \\ &\quad + q_{1122}(u_1^2u_2^2+u_1^2u_3^2+u_2^2u_3^2) \\ V_{\rm B} &= b_1(u_1^2+u_2^2) + b_3u_3^2 + c_{111}(u_1^3+u_2^3) + c_{333}u_3^3 \\ &\quad + q_{1111}(u_1^4+u_2^4) + q_{3333}u_3^4 + q_{1122}u_1^2u_2^2 \\ &\quad + q_{1133}(u_1^2u_3^2+u_2^2u_3^2), \end{aligned} \tag{1}$$

where (u_1, u_2, u_3) is a displacement vector from the equilibrium position of each atom defined on the coordinate system with axes parallel to the crystal axes **a**, **b** and **c** in the present study. $b_i = k_{\rm B}T/(4\pi^2U_{ii})$ in the present case expresses the harmonic potential $V_{\rm H}$ and the other terms express the anharmonic potential $V_{\rm A}$. The anharmonic potential is assumed to be much smaller than $k_{\rm B}T$. Since the AHV represents the vibration of the nucleus, the AHV parameters are expected to be closely related to high-order reflections. Hence, 4*f*-EDD located closer to the nucleus is expected to be strongly affected by AHV. Since there is a strong correlation between harmonic temperature factors and AHV parameters, they were refined alternately. Since the contribution of valence electrons to structure factors is significant in the low-order reflections, but that of the vibration of atoms becomes more in the higher-order reflections, the simultaneous refinement of the parameters of valence electrons and AHV is expected to result in a proper partition of the aspherical EDD among both types of parameters, although it does not guarantee a perfect separation. In MTOT AHV parameters were not refined with the orbital parameters and no information was obtained from the AHV analysis. Therefore, in the present study all AHV parameters were refined with electron-population and kappa parameters simultaneously. The refinement at 430 K was carried out again in the same way and the results at the three temperatures are compared.

3.2. X-ray AO analysis

We refined the X-ray diffraction data by XAO analysis (Tanaka & Ōnuki, 2002; Tanaka *et al.* 2008). This method

[1] Supplementary data for this paper are available from the IUCr electronic archives (Reference: OG5031). Services for accessing these data are described at the back of the journal.

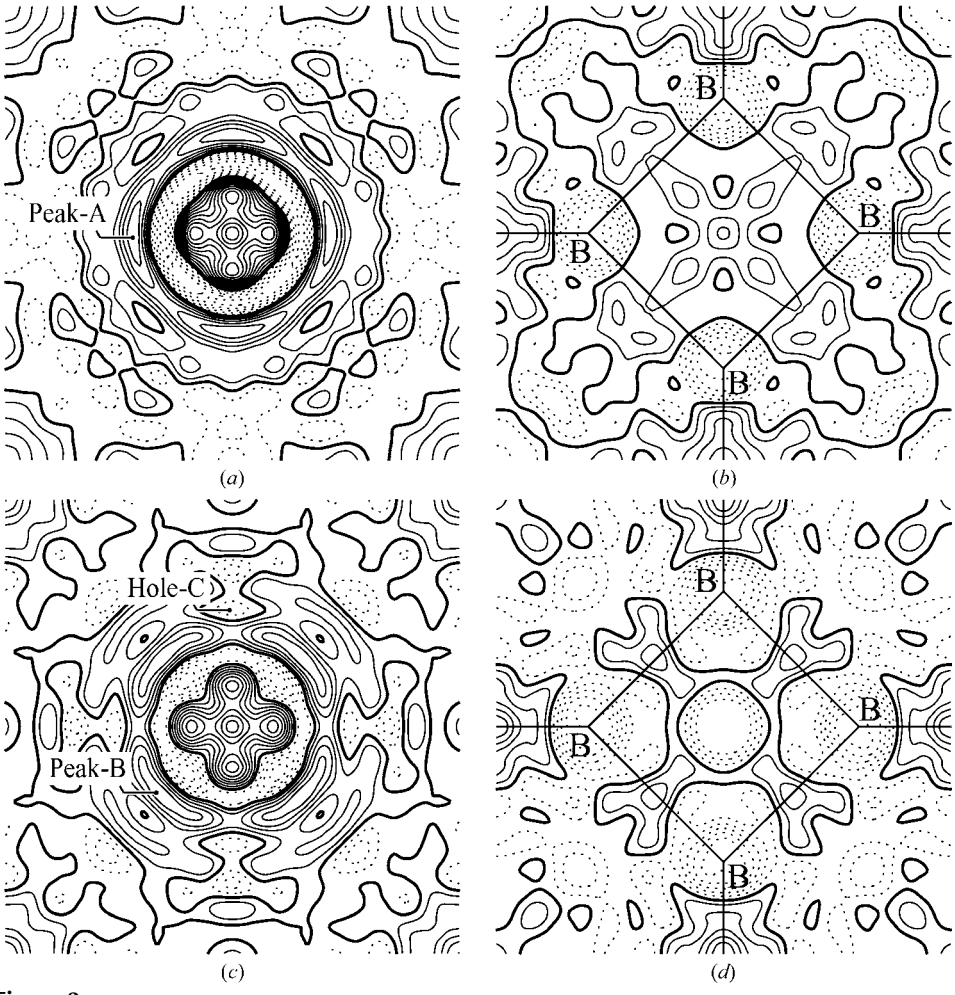

Figure 2
Difference densities (*a*) around Ce at $(\frac{1}{2},\frac{1}{2},\frac{1}{2})$ on the 100 plane at 340 K, (*b*) around B at 340 K, (*c*) Ce at 535 K and (*d*) B at 535 K in spherical refinement. Contours are at intervals of 0.1 e Å^{-3}. Zero contours are drawn as thick lines, positive contours are drawn as thin lines and negative contours are drawn as broken lines.

divides each atom into subshell electrons, which enables us to treat localized electron density quantitatively. Such a quantum-mechanical analysis is useful for investigations of physical properties, since the characteristics of each AO are easily correlated with the observed EDD and thus with the properties of compounds.

3.2.1. Possible orbital models. The EDDs were divided into those of the core and valence electrons, which were further divided into those of the subshell electrons. The 2*s* and 2*p* orbitals of B were assumed to be valence orbitals. For Ce the spin-orbit interaction was taken into account. Since the electron populations of $5p(j = 3/2)$, $5p(j = 1/2)$ and 2*s* tended to exceed full occupation, they were fixed at 1.0, 1.0 and 2.0. The κ parameter of $5p(j = 1/2)$ could not be refined, indicating that $5p(j = 1/2)$ is part of the core orbital. The set of orbitals $5p(j = 3/2)$, $4f(j = 5/2)\Gamma_8$ and $4f(j = 5/2)\Gamma_7$, which is noted as *v*, were commonly refined in all the refinements. The $4f(j = 7/2)$ orbitals were not taken into account since the refinement including $4f(j = 7/2)$ orbitals made the residual densities around Ce and B at 340 K worse and it would not be significant at 535 K. The three kinds of $5d$ orbitals permitted in the O_h crystal field, $5d(j = 3/2)\Gamma_8$, $5d(j = 5/2)\Gamma_8$ and $5d(j = 5/2)\Gamma_7$, and all their different combinations were taken into account in the XAO analysis, since in MTOT at 430 K the peaks along ⟨100⟩ 0.8 Å from Ce were explained as well as those due to the $5d(j = 5/2)\Gamma_8$ orbitals. At 340 and 535 K significant peaks were also observed after refinement *A* along ⟨100⟩ and ⟨110⟩ at 0.9 Å from Ce with heights of 0.4 e Å^{-3}, as shown in Figs. 2(*a*) and (*c*) (see §4.1). The radii of the $4f$ and $5d$ orbitals of Ce (0.38 and 1.15 Å) support the analysis with $5d$ orbitals. In order to confirm that the $5d$ orbitals were occupied by electrons, the refinements without the $5d$ orbitals were first carried out as refinement (*B*). Therefore, the following seven types of valence subshells $(5d(j = 3/2)\Gamma_8)^x$-$(5d(j = 5/2)\Gamma_8)^y(5d(j = 5/2)\Gamma_7)^z$ were assumed in addition to (*A*) and (*B*). Non-zero parameters *x*, *y* and *z* are listed for refinements (*C*) to (*I*) as follows

$$(C)\,v, y;\ (D)\,v, x;\ (E)\,v, z;$$
$$(F)\,v, y, z;\ (G)\,v, x, z;$$
$$(H)\,v, x, y;\ (I)\,v, x, y, z. \qquad (2)$$

Electro-neutrality of the crystal was maintained during the refinement by setting the total sum of the electron populations of each sub-shell orbital equal to that of the positive charges of the nuclei in the unit cell. For example, in refinement (*B*) the following equation was applied

$$g_{\rm Ce}[4n(4f_{j=5/2}\Gamma_8) + 2n(4f_{j=5/2}\Gamma_7) + 4n(5p_{j=3/2}) + 2n(5p_{j=1/2}) + 48] + g_{\rm B}[2n(2p_x) + n(2p_z) + n(2s) + 2] = g_{\rm Ce}Z_{\rm Ce} + g_{\rm B}Z_{\rm B}, \qquad (3)$$

where *g*, *n* and *Z* indicate the multiplicities of the Ce and B atoms in the unit cell, electron population and atomic number. The number in front of the electron population is a degeneracy of each orbital imposed by the crystal symmetry. The point-group symmetry of the B site constrains the *n* and κ values of the $(2p_x)$ and $(2p_y)$ orbitals to be the same. The κ parameters describe expansion/contraction of the orbital.

3.2.2. XAO analysis at 340 K. The populations of the orbitals in each model were refined. When one of them became negative, the model was discarded. In refinements (*F*) and (*G*),

Table 2
Extinction and final parameters at 340 K.

Parameters for B at (0, 0, z), electron populations n, kappa parameter κ, anisotropic temperature factors U^{ij} ($\times 10^{-5}$ Å^2) and b_j ($\times 10^{-19}$ J Å^{-2}), anharmonic cubic parameters c_{ijj} ($\times 10^{-19}$ J Å^{-3}), quartic parameters q_{iijj} ($\times 10^{-19}$ J Å^{-4}), height of peak A $\Delta\rho_A$, maximum peaks in residual density distribution $\Delta\rho_{max}$, height of B in residual density distribution $\Delta\rho_{boron}$. Anisotropic temperature factors are defined as $T_H = \exp(-2\pi^2 \sum_{i,j} yh_i h_j a_i^* a_j^*) U^{ij}$ and anharmonic potentials V are defined in the text. R factors: $R_1 = \Sigma||F_o| - |F_c||/\Sigma|F_o|$, $R_2 = \Sigma(|F_o| - |F_c|)^2/\Sigma|F_o|^2$. Anisotropic type I extinction parameters ($\times 10^4$ s) with Thornley–Nelmes distribution function. The significant AHV parameters are shown in bold. With respect to the refinements, see text in §4.2.

Refinement	Degeneracy	(*A*) SPH	(*B*) without 5*d*	(*C*) $5d(j = 5/2)\Gamma_8$	(*D*) $5d(j = 3/2)\Gamma_8$
R_1		0.00909	0.00767	0.00749	0.00750
R^2		0.01150	0.01022	0.00998	0.00999
Ce					
U^{11}		689 (1)	685 (1)	681 (1)	681 (1)
b_1		681 (1)	686 (1)	689 (1)	689 (1)
n ($4f\ j = 5/2\Gamma_8$)	4	1/6	0.47 (4)	0.53 (4)	0.53 (4)
n ($4f\ j = 5/2\Gamma_7$)	2	1/6	0.00	0.00	0.00
n ($5d\ j = 5/2\Gamma_8$)	4	–	–	0.69 (12)	–
n ($5d\ j = 3/2$)	4	–	–	–	0.75 (13)
κ ($4f\ j = 5/2\Gamma_8$)	4	–	1.52 (6)	1.44 (5)	1.43 (5)
κ ($4f\ j = 5/2\Gamma_7$)	2	–	–	–	–
κ ($5p\ j = 3/2$)	4	–	0.89 (2)	0.90 (3)	0.90 (3)
κ ($5d\ j = 5/2\Gamma_8$)	4	–	–	1.10 (9)	–
κ ($5d\ j = 3/2$)	4	–	–	–	1.08 (9)
q_{1111}		–	**0.6 (3)**	**0.7 (3)**	**0.6 (3)**
q_{1122}		–	**2.8 (8)**	**1.2 (8)**	**1.5 (8)**
$\Delta\rho_A$ (e Å^{-3})		0.59	0.56	0.37	0.45
Valence of Ce		+3.00 (–)	+2.12 (16)	−0.88 (51)	−1.12 (54)
B					
z		0.30062 (20)	0.29901 (231)	0.29923 (145)	0.29929 (145)
U^{11}		525 (6)	513 (5)	518 (5)	518 (5)
U^{33}		345 (9)	343 (9)	331 (7)	330 (7)
b_1		894 (10)	915 (9)	907 (8)	907 (8)
b_3		1362 (36)	1367 (34)	1419 (32)	1421 (32)
n (2*s*)	1	2.00	2.00	2.00	2.00
n ($2p_x$) = n ($2p_y$)	2	1/2	0.25 (4)	0.03 (4)	0.02 (4)
n ($2p_z$)	1	1/2	0.86 (8)	0.79 (8)	0.78 (8)
κ (2*s*)	1	–	1.07 (3)	1.09 (3)	1.09 (3)
κ ($2p_x$) = κ(p_y)	2	–	0.97 (22)	1.20 (35)	1.22 (39)
κ ($2p_z$)	1	–	0.95 (9)	0.95 (9)	0.95 (9)
c_{311}		0.0	**−7.0 (40)**	**−6.3 (43)**	**−6.2 (43)**
c_{333}		0.0	−3.4 (56)	−3.1 (73)	−2.8 (73)
q_{1111}		0.0	−6.8 (76)	−6.6 (74)	−6.3 (74)
q_{3333}		0.0	−8.4 (275)	−20.9 (301)	−18.9 (302)
q_{1122}		0.0	11.5 (383)	14.2 (370)	14.5 (371)
q_{1133}		0.0	**61.4 (558)**	**65.0 (583)**	**61.1 (585)**
Extinction					
Y_{11}		13.9 (5)	15.0 (6)	14.3 (5)	14.4 (6)
Y_{22}		18.4 (13)	19.8 (12)	18.4 (11)	18.0 (11)
Y_{33}		20.0 (13)	22.8 (13)	21.6 (12)	21.4 (13)
Y_{12}		−0.6 (5)	−0.4 (4)	−0.5 (4)	−0.5 (4)
Y_{13}		−3.3 (6)	−3.8 (5)	−3.2 (5)	−3.2 (5)
Y_{23}		0.9 (8)	0.6 (7)	−0.1 (6)	−0.1 (6)
$\Delta\rho_{max}$ (e Å^{-3})		1.17	0.81	0.70	0.70
$\Delta\rho_{boron}$ (e Å^{-3})		−0.52	−0.43	−0.39	−0.39

the electron population of $5d(j = 5/2)\Gamma_7$ orbitals became negative and models (*F*) and (*G*) were discarded. When the populations of $5d(j = 5/2)\Gamma_8$, $5d(j = 5/2)\Gamma_7$ and $5d(j = 3/2)$ were refined simultaneously in refinement (I), correlation among them was extremely large and they became negative, except that of $5d(j = 3/2)$ reducing refinement (*I*) to (*D*).

Since the correlation coefficient between the populations of $5d(j = 5/2)\Gamma_8$ and $5d(j = 3/2)\Gamma_8$ orbitals is −0.96 in refinement (*H*), the errors of their electron populations were so large that the values became insignificant. Hence, they were refined separately and refinement (*H*) was divided into refinements (*C*) and (*D*). On the other hand, in refinement (*E*) $5d(j = 5/2)\Gamma_7$ orbitals were fully occupied, however, improvement of the residual densities and a decrease in the *R* factors were not observed. Therefore, acccurate X-ray measurement of the EDD at 340 K limited the possible electron configuration to (*C*) and (*D*). Refinements (*B*)–(*D*) will be compared in the forthcoming discussion.

3.2.3. XAO analysis at 535 K. Refinement (*I*) at 535 K was reduced to refinement (*D*), and (*H*) was reduced to (*C*) and (*D*) for the same reason as described in §3.2.2. At this stage we cannot discriminate between the other refinements at 535 K.

3.3. Parameter interactions between κ and other parameters

In the least-squares refinement for the system with highly condensed electrons like the present compound, parameter interactions should be carefully treated. Usually parameters with a similar effect on the EDD have severe parameter interactions with each other. When they are refined simultaneously, their parameters oscillate or they do not converge well. In these cases they were refined separately. There are many parameter interactions besides that between AHV parameters and harmonic temperature factors. The κ parameters have a strong correlation with the other parameters. When the scale factor and κ parameter of 4*f* orbitals were refined together, the height of the residual peak on Ce became 1.4–3.0 times larger than when they were refined separately, even though the correlation coefficients are not large. When κ parameters of 4*f* orbitals were added to the refinement, the correlation between the population of the 4*f* orbitals and the scale factor became important (coefficients between −0.55 and −0.94). Since the correlation coefficients at 340 K in refinements (*C*) and (*D*) between κ of $5p(j = 3/2)$ and those of 5*d* orbitals were −0.93 and −0.97, and these parameters oscillated, they were refined separately. Other examples are those between κ parameters of the B $2p_x(= 2p_y)$ and B 2*s* orbitals, between κ parameters and the electron population of the B $2p_x(= 2p_y)$ orbitals *etc.*

Table 3
Extinction and final parameters at 535 K.

Height of peak B $\Delta\rho_B$, $E(5d\text{-}t_{2g})$ and $E(5d\text{-}e_g)$ is the energy levels calculated by the program *WAVE*03 (Tanaka *et al.*, 2008). With respect to the refinements, see text in §4.3. Details are the same as given in Table 2.

Refinement	Degeneracy	(*A*)SPH	(*B*) without 5*d* orbitals	(*C*) $5d(j = 5/2)\Gamma_8$	(*D*) $5d(j = 3/2)\Gamma_8$	(*E*) $5d(j = 5/2)\Gamma_7$	(*F*) $5d(j = 5/2)\Gamma_8 + 5d(j = 5/2)\Gamma_7$	(*G*) $5d(j = 3/2)\Gamma_8 + 5d(j = 5/2)\Gamma_7$
R_1		0.01030	0.00935	0.00878	0.00875	0.00902	0.00873	0.00875
R_2		0.01267	0.01146	0.01060	0.01041	0.01078	0.01040	0.01042
Ce								
U^{11}		1087 (2)	1079 (2)	1079 (2)	1080 (2)	1080 (2)	1079 (2)	1079 (2)
b_{11}		680 (1)	685 (1)	685 (1)	685 (1)	684 (1)	684 (1)	685 (1)
n ($4f\ j = 5/2\Gamma_8$)	4	1/6	0.27 (6)	0.47 (7)	0.49 (7)	0.37 (7)	0.49 (7)	0.49 (8)
n ($4f\ j = 5/2\Gamma_7$)	2	1/6	0	0	0	0	0	0
n ($5d\ j = 5/2\Gamma_8$)	4	–	–	1.00	–	–	0.72 (13)	–
n ($5d\ j = 5/2\Gamma_7$)	2	–	–	–	–	1.00	1.00	0.41 (25)
n ($5d\ j = 3/2$)	4	–	–	–	1.00	–	–	1.00
κ ($4f\ j = 5/2\Gamma_8$)	4	–	1.60 (21)	1.38 (9)	1.36 (8)	1.47 (13)	1.33 (9)	1.32 (8)
κ ($4f\ j = 5/2\ \Gamma_7$)	2	–	–	–	–	–	–	–
κ ($5p\ j = 3/2$)	4	–	0.91 (4)	0.92 (7)	0.92 (3)	0.92 (5)	0.91 (8)	0.92 (5)
κ ($5d\ j = 5/2\ \Gamma_8$)	4	–	–	1.17 (18)	–	–	1.19 (30)	–
κ ($5d\ j = 5/2\ \Gamma_7$)	2	–	–	–	–	1.16 (21)	1.15 (21)	1.14 (59)
κ ($5d\ j = 3/2$)	4	–	–	–	1.17 (9)	–	–	1.14 (9)
q_{1111}		–	**−0.6 (1)**	−0.1 (1)	−0.1 (1)	**−0.3 (1)**	−0.1 (1)	−0.1 (1)
q_{1122}		–	**1.9 (4)**	**1.3 (4)**	**1.3 (4)**	**1.8 (4)**	**1.3 (4)**	**1.3 (4)**
$\Delta\rho_B$ (e Å^{-3})		0.48	0.47	0.40	0.37	0.39	0.33	0.33
Valence of Ce		+3.00 (–)	+2.92 (24)	−1.88 (28)	−1.96 (28)	+0.52 (28)	−2.84 (59)	−2.78 (59)
$E(5d\ t_{2g})$ (a.u.)		+0.023	–	–	–	–	−0.022	−0.022
$E(5d\ e_g)$ (a.u.)		−0.035	–	–	–	–	+0.33	+0.33
B								
z		0.30085 (2)	0.30208 (278)	0.30186 (159)	0.30194 (158)	0.30186 (162)	0.30191 (158)	0.30193 (159)
U^{11}		742 (7)	733 (7)	738 (7)	737 (7)	736 (7)	736 (6)	736 (6)
U^{33}		419 (10)	407 (9)	407 (9)	407 (9)	409 (9)	409 (9)	409 (9)
b_{11}		996 (9)	1008 (9)	1002 (9)	1002 (9)	1003 (9)	1003 (8)	1003 (8)
b_{33}		1763 (40)	1815 (42)	1813 (41)	1814 (41)	1806 (41)	1805 (39)	1807 (39)
n ($2s$)	1	2.00	2.00	2.00	2.00	2.00	2.00	2.00
n ($2p_x$) = n ($2p_y$)	2	1/2	0.47 (7)	0.00	0.00	0.23 (7)	0.00	0.00
n ($2p_z$)	1	1/2	0.55 (15)	0.68 (5)	0.68 (5)	0.62 (15)	0.53 (10)	0.54 (10)
κ ($2s$)	1	–	1.04 (4)	1.07 (3)	1.07 (3)	1.04 (4)	1.07 (3)	1.07 (3)
$\kappa(2p_x) = \kappa(2p_y)$	2	–	0.65 (6)	–	–	0.76 (15)	–	–
κ ($2p_z$)	1	–	0.92 (15)	0.92 (9)	0.92 (10)	0.92 (13)	0.93 (15)	0.93 (14)
c_{311}		0.0	**5.0 (32)**	**4.3 (32)**	**4.5 (32)**	**4.4 (33)**	**4.5 (32)**	**4.5 (32)**
c_{333}		0.0	3.6 (87)	2.7 (94)	3.1 (94)	2.7 (96)	2.9 (93)	3.0 (94)
q_{1111}		0.0	**−6.6 (40)**	**−5.1 (39)**	**−5.0 (38)**	**−5.2 (40)**	**−5.1 (39)**	**−5.2 (39)**
q_{3333}		0.0	9.0 (196)	10.9 (196)	11.1 (195)	9.3 (198)	11.2 (192)	10.6 (194)
q_{1122}		0.0	**52.8 (197)**	**46.7 (192)**	**46.3 (192)**	**44.9 (197)**	**46.8 (192)**	**46.8 (193)**
q_{1133}		0.0	−21.4 (345)	−11.9 (343)	−13.8 (341)	−14.3 (348)	−15.2 (342)	−15.9 (343)
Extinction								
Y_{11}		15.4 (16)	17.6 (19)	16.1 (14)	15.7 (13)	16.4 (16)	15.8 (13)	15.7 (13)
Y_{22}		12.3 (14)	14.3 (18)	14.3 (15)	13.9 (14)	14.0 (16)	13.7 (14)	13.6 (14)
Y_{33}		9.2 (5)	9.8 (6)	8.4 (5)	8.5 (5)	9.4 (6)	8.2 (5)	8.3 (4)
Y_{12}		−0.2 (9)	−0.7 (10)	−0.6 (8)	−0.7 (8)	−0.8 (9)	−0.8 (8)	−0.8 (8)
Y_{13}		−0.9 (6)	−1.5 (6)	−1.6 (5)	−1.6 (5)	−1.6 (5)	−1.6 (4)	−1.6 (5)
Y_{23}		−2.5 (6)	−3.0 (7)	−2.4 (5)	−2.4 (5)	−2.7 (6)	−2.3 (5)	−2.3 (5)
$\Delta\rho_{max}$ (e Å^3)		0.70	0.54	0.50	0.50	0.52	0.55	0.54
$\Delta\rho_{boron}$ (e Å^{-3})		−0.58	−0.45	−0.33	−0.33	−0.40	−0.32	−0.32

4. Result and discussion

4.1. Spherical-atom model (refinement *A*) at 340 and 535 K

Parameters after the spherical-atom refinement (refinement *A*) are listed in Tables 2(*a*) and 3(*a*) at 340 and 535 K. The residual densities around Ce and B at 340 K are shown in Figs. 2(*a*) and (*b*), and those at 535 K in Figs. 2(*c*) and (*d*). In order to understand the difference densities the $4f\Gamma_7$ and $5d\Gamma_7$ orbitals must extend along the ⟨110⟩ and ⟨111⟩ directions, and Γ_8 orbitals extend to ⟨100⟩ directions. Since no aspherical EDD is introduced in the atomic scattering factors, these figures exhibit the experimental and unbiased aspherical EDD.

The positive peak on Ce and those extending along the ⟨100⟩ directions near Ce in Figs. 2(*a*) and (*c*) have peak heights of 0.8 and 0.6 e Å^{-3}. The directions of these peaks in the vicinity of Ce indicate that the electron population of $4f(j = 5/2)\Gamma_8$ is larger than those of $4f(j = 5/2)\Gamma_7$ at 340 and 535 K, which contradicts the results at 430 K but agrees with those at room temperature. Negative values, −0.4 e Å^{-3}, near Ce along the ⟨110⟩ directions in Fig. 2(*c*) at 535 K seem to be due to the $4f$-Γ_7 orbitals. Negative peaks surround these positive

peaks almost spherically in Figs. 2(*a*); these features were not observed at 430 K (MTOT).

Outside the negative area there are positive areas mainly correlated to the 5*d* electrons described in the previous section. The positive peaks along the ⟨100⟩ and ⟨110⟩ directions at 0.9 Å from Ce with a height of 0.4 e Å^{-3} are shown in Figs. 2(*a*) and (*c*). They are hereinafter referred to as peak A and peak B, and their peak heights are listed as $\Delta\rho_A$ and $\Delta\rho_B$ in Tables 2 and 3. The positive peaks along the ⟨100⟩ directions in Fig. 2(*a*) correspond to $5d(j = 5/2)\Gamma_8$ orbitals which were also found in MTOT at 430 K. Fig. 2(*a*) shows that $4f(j = 5/2)\Gamma_8$ and $5d(j = 5/2)\Gamma_8$ orbitals are expected to be occupied in spite of the electron repulsion between them, which is different from our previous results at 430 K. This will be discussed in the forthcoming section.

The positive peaks on the B—B_{out} bond between the B_6 octahedra (B $2p_z$ orbitals) in Figs. 2(*b*) and (*d*), which are due to the two-centre electrons on the B—B covalent bonds, are higher than those near the B—B bonds in the B_6 octahedra. On the other hand, heights of the negative peaks on the B atom denoted as $\Delta\rho_{boron}$ are listed in Tables 2 and 3. The peaks on B with a height of −0.5 e Å^{-3} are expected to be correlated to the number of 2*p* electrons. Thus, as was observed at 430 K the electron population of the B $2p_x(= 2p_y)$ orbital is expected to be less than the 0.5 e assumed in refinement (*A*).

4.2. XAO analysis at 340 K

Parameters after refinements (*B*), (*C*) and (*D*) are listed in Table 2 and the residual densities around Ce are shown in Figs. 3(*a*) to (*c*). R_1 and R_2 before these refinements, but after the AHV analysis, are 0.00892 and 0.01142. The harmonic temperature factors of Ce are larger than those of B, which were also observed at 430 K since the framework of the B_6 octahedra is firm and B is not as mobile as Ce located at the centre of the unit cell, although the B_6 moiety does lose electrons (which is clear from Table 2). However, the AHV parameters of Ce are small and those of B are one order larger than those of Ce. This tendency does not change in refinements (*C*) and (*D*).

The residual density around the B atom after refinement (*C*), which is almost the same as that after refinement (*D*), is illustrated in Fig. 3(*d*). That after refinement (*B*) is not shown since it is almost the same as that of refinement (*A*) shown in Fig. 2(*b*), except for the reduction of the negative peaks on B as listed in Tables 2(*a*) and (*b*). The hole of −0.52 e Å^{-3} on the B atom in Fig. 2(*d*) shifts towards the inside of the B_6 frame with a height of −0.39 e Å^{-3} in Fig. 3(*d*). After refinements (*B*)–(*D*) the electron populations of $4f(j = 5/2)\Gamma_7$ orbitals became zero, but those of the $4f(j = 5/2)\Gamma_8$ orbitals increased by electron transfer from B $2p_x(= 2p_y)$ orbitals. It makes the total electron populations of the 4*f* orbitals close to 2.0, ranging from 1.88 (16) to 2.12 (16) as listed in Table 2. On the other hand, B 2*s* is fully occupied and the populations of $2p_z$ increased from 0.5 to 0.79 (8) and 0.78 (8), which are equal within experimental error after refinements (*B*) to (*D*). The peaks of the B—B_{out} bonds on the residual density map are also large, but they were reduced from 0.45 to 0.32 e Å^{-3}. The height of the highest residual peak $\Delta\rho_{max}$ in Table 2 is that on Ce. These results show that electrons are transferred from B $2p_x$ (= p_y) orbitals to Ce 4*f* and 5*d* orbitals.

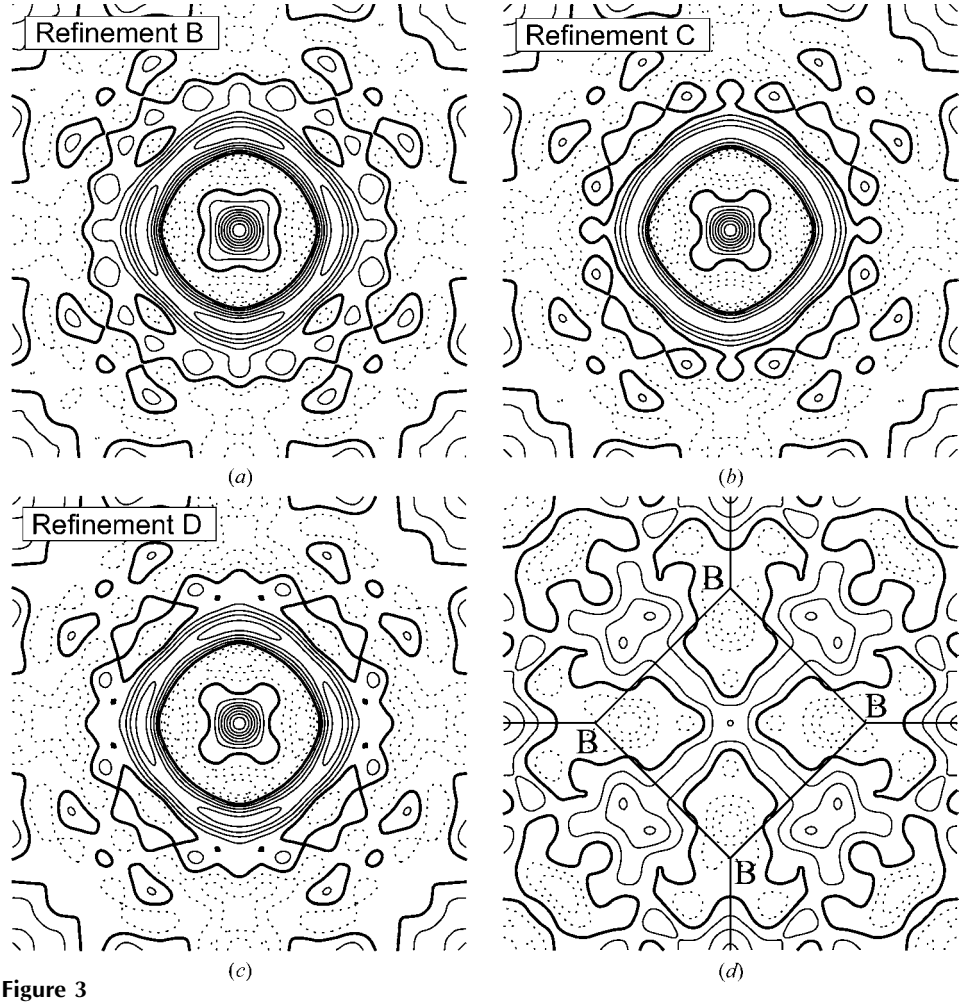

Figure 3
Residual densities around (*a*) Ce after refinement (*B*), (*b*) Ce after refinement (*C*), (*c*) Ce after refinement (*D*) and (*d*) B after refinement (*C*). Contours are as in Fig. 2.

4.2.1. Comparison of the electron configurations obtained by

refinements (*B*) to (*D*). Now we discuss which analysis gives the best electronic configuration. The criteria are:

(i) the *R* factor,

(ii) the height of peak A ($\Delta\rho_{\rm A}$),

(iii) the residual density around B ($\Delta\rho_{\rm boron}$) and

(iv) the physical validity.

Before discussing the electron configurations, it is necessary to comment on the improvement of the *R* factors and EDD. Since the ratio of the number of 4*f* electrons to the total number of electrons in the unit cell is almost 1% and accordingly the contribution of the aspherical EDD of localized 4*f* and 5*d* orbitals to structure factors is very small, and the *R* factor after spherical refinement (*A*) at both temperatures is close to 1%, the reduction of the *R* factors even by only 0.1% can be a good measure of the validity of the refinement. The mean radius of the 5*d* orbitals is 2.71 a.u. and that of 4*f* is 0.983 a.u. (Mann, 1968). The reduction of 5*d* peaks seems to be approximately $(2.71/0.983)^2 = 7.6$ times more significant than that of 4*f*. Therefore, the reduction of 5*d* peak heights by 0.1 e Å^{-3} is very large. In the present study the highly localized 4*f*-EDD is explained well and almost all the aspherical peaks have disappeared. However, peaks and holes of 5*d* EDD are distributed in a rather diffuse way and it becomes necessary to realise where the peaks owing to 5*d* electrons appear on the difference-density map. Therefore, the EDD of $5d(j = 5/2)\Gamma_8$ orbitals, $\Delta\rho_{5d}$, is calculated as

$$\Delta\rho_{5d} = \left(\frac{1}{V}\right)\sum\left[F_{\rm calc}(\mathbf{k}) - F_{{\rm calc}-5d}(\mathbf{k})\right]\exp(i\mathbf{k}\cdot\mathbf{r}), \quad (4)$$

where *V* is the volume of the unit cell and **k** is a scattering vector. $\Delta\rho_{5d}$ with a height of 0.22 e Å^{-3} extending along the ⟨100⟩ direction is illustrated in Fig. 4. It is evident that the peaks outside the spherical valley surrounding Ce in Fig. 2(*a*), including peak A, are closely correlated to 5*d* EDD. $5p(j = 3/2)$ peaks calculated in the same way appear just a little inside $\Delta\rho_{5d}$, but overlap significantly. However, the population and κ parameter are stable and do not change throughout the refinements. Therefore, the peaks in the outside ring of Fig. 2(*a*) can be assumed to be due to 5*d* electrons and the area with 5*d* peaks is called the 5*d* area hereinafter.

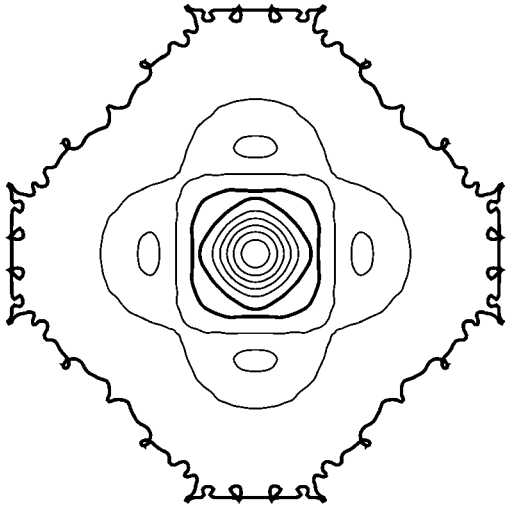

Figure 4
The EDD of $5d(j = 5/2)\Gamma_8$ orbitals. See text. Contours are as in Fig. 2.

The populations of the 4*f* orbitals of the three refinements in Table 2 are approximately equal to each other and the peaks at 0.8 e Å^{-3} extending along ⟨100⟩ in Fig. 2(*a*) vanished. Therefore, the aspherical EDD due to $4f$-Γ_8 orbitals are explained fairly well. Although the *R* factor and $\Delta\rho_{\rm boron}$ of refinement (*B*) in Table 2(*b*) are improved from refinement (*A*), $\Delta\rho_{\rm A}$ of refinement (*B*) in Table 2(*b*) is evidently higher than those of the other refinements. These facts show that the 5*d* orbitals are occupied and the refinement including 5*d* orbitals is essential, and refinement (*B*) is rejected.

Refinements (*C*) with $5d(j = 5/2)\Gamma_8$ and (*D*) with $5d(j = 3/2)\Gamma_8$ are now compared. Since the $\Delta\rho_{\rm A}$ of refinement (*C*) is ~ 0.1 e Å^{-3} smaller than that of refinement (*D*) and the 5*d* area with a height greater than 0.4 e Å^{-3} is wider in refinement (*D*), refinement (*C*) seems to be better than refinement (*D*). Since fourfold degenerate $5d(j = 3/2)$ orbitals are equally occupied in the crystal field O_h, the density of $5d(j = 3/2)\Gamma_8$ electrons is always spherical. On the other hand, the EDD of $5d(j = 5/2)\Gamma_8$ extends toward the ⟨100⟩ direction, as illustrated in Fig. 5 in MTOT. Therefore, the authors conclude that model (*C*) is the closest to the electron configuration of Ce at 340 K among the electron configurations examined.

The result of refinement (*C*) indicates that electrons are transferred from B $2p_x(= p_y)$ orbitals to $5d(j = 5/2)\Gamma_8$ orbitals accompanying the increase of the total 4*f* electron population from 0.92 (11) at 298 K (Tanaka & Ōnuki, 2002) to 2.12 (16) in refinement (*C*). It shows that electrons are transferred from B $2p_x(= p_y)$ orbitals to Ce 4*f* orbitals directly or *via* Ce $5d(j = 3/2)\Gamma_8$ and/or $5d(j = 5/2)\Gamma_8$ orbitals. Since the energy levels of 5*d* orbitals are much closer to B 2*p* than 4*f* orbitals, as was stated in the previous section, the probability of the transfer from B $2p_x(= p_y)$ to Ce $5d(j = 3/2)$ and/or $5d(j = 5/2)\Gamma_8$, and then to $4f(j = 5/2)\Gamma_8$ orbitals is expected to be larger than the direct transfer. Since the $4f(j = 5/2)\Gamma_8$ and $5d(j = 5/2)\Gamma_8$ orbitals have different parities and extend exactly to the same directions, the transition moment between them is expected to be the largest.

The $5d(j = 5/2)\Gamma_8$ orbitals are partially and fully occupied at 340 and 430 K, but $4f(j = 5/2)\Gamma_8$ orbitals are more populated than $4f(j = 5/2)\Gamma_7$ orbitals at 340 K, in contrast to the results at 430 K in MTOT. At 430 K, the full occupation of $5d(j = 5/2)\Gamma_8$ orbitals maximizes the electric repulsion between $4f(j = 5/2)\Gamma_8$ and $5d(j = 5/2)\Gamma_8$ orbitals and makes the energy level of the $4f$-Γ_8 orbitals higher than that of the $4f$-Γ_7 orbitals. The partial and full occupation of $5d(j = 5/2)\Gamma_8$ orbitals at 340 and 430 K seems to make such a difference. The partial occupation at 340 K is a transient state between 298 K with no 5*d* electrons and 430 K with fully occupied 5*d* orbitals.

4.3. XAO analysis at 535 K

Parameters from refinements (*B*)–(*G*) are listed in Table 3 and the residual densities around Ce are shown in Figs. 5(*a*)–(*e*). R_1 and R_2 after AHV refinement, but before the XAO

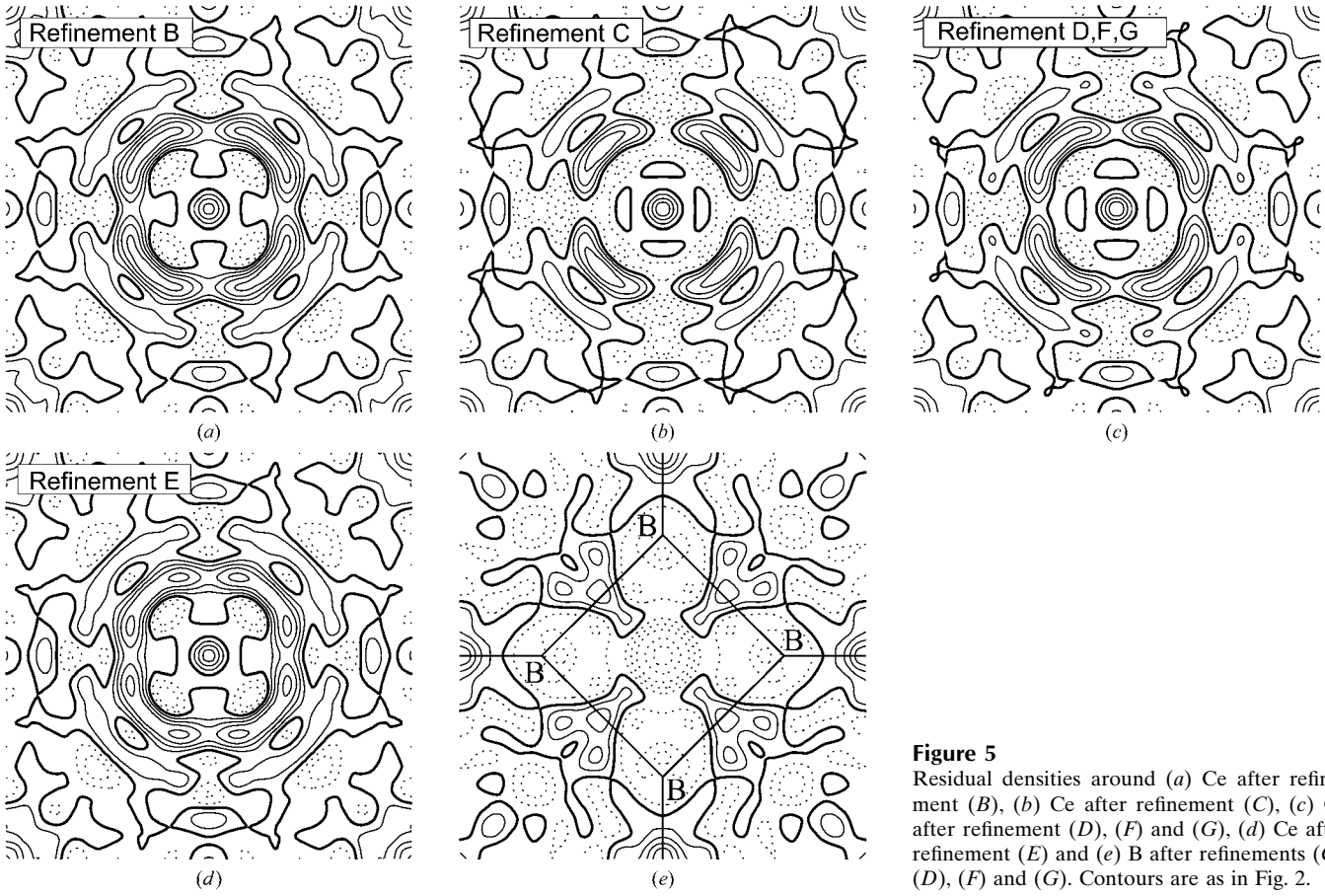

Figure 5
Residual densities around (*a*) Ce after refinement (*B*), (*b*) Ce after refinement (*C*), (*c*) Ce after refinement (*D*), (*F*) and (*G*), (*d*) Ce after refinement (*E*) and (*e*) B after refinements (*C*), (*D*), (*F*) and (*G*). Contours are as in Fig. 2.

analysis, were 0.01024 and 0.01265. Most of the AHV parameters q_{1111} and q_{1122} of Ce are significant at 535 K. Since the residual densities around Ce after refinements (*F*) and (*G*) are similar to those after refinement (*D*), only those after refinements (*B*), (*C*), (*D*) and (*E*) are shown in Figs. 5(*a*)–(*d*). The difference density after refinement (*B*) is similar to that of refinement (*A*) in Fig. 2(*d*) except for the reduction of the depths of the holes on B, $\Delta\rho_{\rm boron}$, listed in Tables 3(*a*) and (*b*). Since the difference density around the B atom after refinements (*C*)–(*D*) are almost the same, only that after refinement (*C*) is shown in Fig. 5(*e*). The hole in B was improved in the same way as that described in §4.2 at 340 K. However, the peaks on the B—$B_{\rm out}$ bonds remain the highest in the residual density in all refinements (*B*)–(*G*). The heights $\Delta\rho_{\rm max}$ are listed in Table 3.

In all the refinements the electron population of the $4f(j = 5/2)\Gamma_7$ orbitals became zero. The populations of B $2p_x$ (= p_y) orbitals were also zero, except for refinements (*B*) and (*E*). As listed in Table 3 the total number of electron populations of 4*f* orbitals range from 1.08 (24) to 1.96 (32) and the population of B $2p_z$ is greater than the formal charge of 0.5. This indicates that electrons are transferred from B $2p_x$ (= p_y) orbitals to Ce 4*f* and 5*d* orbitals, as was seen at 340 and 430 K.

4.3.1. Comparison of the electron configurations obtained by refinements (*B*)–(*G*). Refinements (*B*) and (*E*) are not good judging from the higher *R* factors than those of the other refinements, although they are reduced significantly from those of refinement (*A*). Furthermore, peak B in Figs. 5(*a*) and (*d*) was not reduced significantly from that in Fig. 2(*c*), and $\Delta B_{\rm boron}$ in Table 3 was reduced less than those of the others. Therefore, the results of refinement (*B*) and (*E*) are discarded although the peaks on Ce are reduced significantly, which is the main reason for the 0.00095 and 0.00128 reduction of the *R* factors from 0.0103 for refinements (*B*) and (*E*).

The remaining refinements (*C*), (*D*), (*F*) and (*G*) are now compared. The final parameters, except for configurations of the 5*d* electrons, are equal within experimental error, and the *R* factors and the residual density around the B atoms do not differ significantly among them. The height of peak B, $\Delta\rho_{\rm B}$, in Table 3 became smallest after refinement (*F*) and (*G*), although the difference is negligible. Negative peaks of -0.15 e Å^{-3} are found in Fig. 2(*c*) in the 5*d* area along the ⟨100⟩ directions at 1.0 Å from Ce. They are called hole C hereafter. It deepened to -0.33 e Å^{-3} in Fig. 5(*b*) after refinement (*C*). Since no 5*d* orbitals are included in refinement (*A*) and the $5d(j = 5/2)\Gamma_8$ orbitals extending to ⟨100⟩ are the only 5*d* orbitals included in refinement (*C*), hole C in Fig. 5(*b*) can be assigned to them and the difference in the depth of hole C corresponds to the peak height of the fully occupied $5d(j = 5/2)\Gamma_8$ orbitals. Therefore, it may be appropriate to exclude refinement (*C*) from further discussion. We should note again that even the fully occupied 5*d* orbitals can produce a small difference in the 5*d* area. Since there is actually no difference in the residual densities of refinements (*D*), (*F*) and (*G*), it is

Table 4
Final parameters at 340, 430 and 535 K.

	(1)	(2)	(3)
Temperature (K)	340	430	535
R_1	0.007	0.011	0.009
R_2	0.010	0.014	0.010
Ce			
U^{11}	681 (1)	847 (2)	1079 (2)
$b11$	689 (1)	701 (2)	684 (1)
n ($4f\ j = 5/2\Gamma_8$)	0.53 (4)	0.10 (14)	0.49 (7)
n ($4f\ j = 5/2\Gamma_7$)	0.00	0.61 (23)	0.00
n ($5d\ j = 5/2\Gamma_8$)	0.69 (12)	1.00	0.72 (13)
n ($5d\ j = 5/2\Gamma_7$)	–	–	1.00
κ ($4f\ j = 5/2\Gamma_8$)	1.44 (5)	1.28 (23)	1.33 (9)
κ ($4f\ j = 5/2\Gamma_7$)	–	1.45 (14)	–
$\kappa(5p\ j = 3/2)$	0.90 (3)	0.89 (4)	0.91 (8)
κ ($5d\ j = 5/2\Gamma_8$)	1.10 (9)	1.12 (11)	1.19 (30)
$\kappa(5d\ j = 5/2\Gamma_7)$	–	–	1.15 (21)
q_{1111}	**0.7 (3)**	−0.3 (6)	−0.1 (1)
q_{1122}	**1.2 (8)**	**2.6 (18)**	**1.3 (4)**
Valence of Ce	−0.88 (51)	−1.62 (72)	−2.84 (59)
B			
z	0.29923 (145)	0.30223 (240)	0.30191 (158)
U^{11}	518 (5)	613 (7)	736 (6)
U^{33}	331 (7)	366 (9)	409 (9)
b_{11}	907 (8)	968 (10)	1003 (8)
b_{33}	1419 (32)	1622 (39)	1805 (39)
$n(2s)$	2.00	2.00	2.00
n ($2p_x$) = n ($2p_y$)	0.03 (4)	0.0	0.0
n ($2p_z$)	0.79 (8)	0.73 (12)	0.53 (10)
$\kappa(2s)$	1.09 (3)	0.99 (4)	1.07 (3)
$\kappa(2p_x) = \kappa(2p_y)$	1.2(35)	–	–
κ ($2p_z$)	0.95 (9)	0.90 (10)	0.93 (15)
c_{311}	**−6.3 (43)**	−1.3 (57)	**4.5 (32)**
c_{333}	−3.1 (73)	10.7 (131)	3.0 (94)
q_{1111}	−6.6 (74)	**−10.9 (78)**	**−5.1 (39)**
q_{3333}	−20.9 (301)	**−126.8 (359)**	11.2 (192)
q_{1122}	14.2 (370)	**−84.1 (39)**	**46.8 (192)**
q_{1133}	**65.0 (583)**	**246.1 (645)**	−15.2 (342)

difficult to conclude from the experiment at 535 K which one of the three models is the best. More accurate data measurement is necessary.

However, it is worthwhile to discuss the physical validity of each model. The difference density in Fig. 2(*c*) after the spherical atom refinement (*A*) can be taken as experimental fact, as was discussed in §4.1, and the directional characteristics of the 5*d* area in Fig. 2(*c*) should be explained. As stated in the previous discussion $5d(j = 3/2)\Gamma_8$ orbitals in the O_h crystal field always form a spherical EDD. Thus, refinement (*D*) may not be appropriate to explain the peaks along the ⟨110⟩ direction in the 5*d* area in Fig. 2(*c*). Let us examine the difference between models (*F*) and (*G*). Since the sum of the equally occupied $5d(j = 5/2)\Gamma_8$ and Γ_7 orbitals with the same κ parameter also produce a spherical EDD, the net components along the ⟨110⟩ directions in refinements (*F*) and (*G*) are those of $5d(j = 5/2)\Gamma_7$ with 0.28 (= 1.0–0.72) and 0.41 electrons. However, hole C along ⟨100⟩ and peak B along ⟨110⟩ of refinement (*F*) and (*G*) have almost the same heights as well as *R* factors. Since the XAO analysis fits the superimposed EDD of all the AOs of each atom to the observed one and explains the aspherical EDD, further discrimination between refinements (*F*) and (*G*) may not be possible from the EDD alone. The AHV parameters may be used to discriminate the refinements and will be discussed in §5.2.

4.3.2. Energy levels of 5*d* orbitals at 535 K. $5d(j = 5/2)\Gamma_7$ are more populated than $5d(j = 5/2)\Gamma_8$ in refinement (*F*), but they are less populated than $5d(j = 3/2)\Gamma_8$ orbitals in refinement (*G*), as listed in Table 3. These facts contradict the energy-level diagram shown in Fig. 1(*a*). It is worthwhile to discuss the reason for the occupation of the orbitals which were expected to have higher energy and to examine the possible relationships of the energy levels of atomic orbitals expected from the experimental electron populations of the relevant atoms.

The energy levels of the Ce 5*d* orbitals, $E(5d\text{-}t_{2g})$ and $E(5d\text{-}e_g)$, in the strong crystal field model are listed in Table 3, which were calculated using the program *WAVE*03 (K. T., see also Tanaka *et al.*, 2008), based on the method by Kamimura *et al.* (1969) using a point charge calculated from the populations in Table 3 to compare the strength of the crystal fields. Since the valences of Ce in Table 3 are −2.84 (59) and −2.78 (59) after refinements (*F*) and (*G*), the B atoms are positively charged. In addition, the $2p_x$ (= $2p_y$) orbital of B which is located closest to Ce among the *p* orbitals of B has a small electron population. Thus, the crystal field of Ce in the positively charged B_6 is at least made weaker by the electron transfer and the effect of the neighbouring more negatively charged Ce atoms along the ⟨100⟩ direction becomes stronger. Hence, the energy levels of the $5d\text{-}e_g$ orbitals may lie higher than those of $5d\text{-}t_{2g}$, indicating that the energy levels of the $5d(j = 5/2)\Gamma_8$ orbitals become higher than those of the other 5*d* orbitals, as shown in Fig. 1(*b*).

Since the total number of 4*f* electrons after refinements (*F*) and (*G*) is larger than 1.0 [1.96 (28) and 1.96 (32)], electrons are transferred from B $2p_x$ (= $2p_y$) to Ce 4*f* orbitals directly or *via* the 5*d* orbitals. The transfer of electrons from B 2*p* to Ce 4*f* *via* 5*d* orbitals which have energy closer to B 2*p* than the 4*f* orbitals is the most probable process according to the perturbation theory. Since no population was found on $4f(j = 5/2)\Gamma_7$, as listed in Table 3, a transition *via* the orbitals with Γ_8 symmetry in Fig. 1(*b*) is proposed which we think fits our present results, although we cannot claim that this is the only solution.

5. Comparison of the results at 340, 430 and 535 K

The relationship between the electron configurations and significant AHV parameters at 340 K (refinement *C*), 430 K [see Table 4 column (2)] and at 535 K (represented by refinement *F*) are listed in Table 4 columns (1)–(3). The parameters at 430 K were analyzed again and all AHV parameters were refined with the orbital parameters, as was done in the present study. The population parameters, $n(4f_{j = 5/2}\Gamma_7)$ and $n(4f_{j = 5/2}\Gamma_8)$ in Table 4(*b*) increased from 0.37 (11) in MTOT to 0.61 (23) and from 0.06 (2) to 0.10 (14). However, the ratio of $n(4f_{j = 5/2}\Gamma_7)$ and $n(4f_{j = 5/2}\Gamma_8)$, the energy gap of $4f(j = 5/2)\Gamma_8$ and Γ_7 orbitals and the basic relationships found in MTOT, *i.e.* the fully occupied $5d(j = 5/2)\Gamma_8$ and population

inversion between $4f(j = 5/2)\Gamma_7$ and $4f(j = 5/2)\Gamma_8$ orbitals, were not altered.

5.1. Electron configuration

Figs. 6(*a*)–(*c*) show a bird's-eye view of the difference densities drawn after spherical-atom refinement assuming Ce^{3+} and $B^{0.5-}$ at 340, 430 and 535 K. They all show 4*f* peaks at and around the Ce nucleus and after passing the valley there are hills of 5*d* peaks surrounding the 4*f* peaks. The depths of the valleys in Figs. 6(*a*)–(*c*) are −0.53, −0.20 and −0.46 e Å^{-3}. However, it is very interesting that the combination of the directions of the peak of 4*f* and 5*d* EDD are different. The directions of 4*f* and 5*d* orbitals are both along the ⟨100⟩ directions at 340 K. However, at 430 K 4*f* and 5*d* lobes are located along ⟨110⟩ and ⟨100⟩, and at 535 K along the ⟨100⟩ and ⟨110⟩ directions.

The spherical-atom refinements at the three temperatures exhibit clearly that the directions of the 4*f* peaks near Ce in Figs. 6(*a*) and (*c*) are mainly due to $4f(j = 5/2)\Gamma_8$ orbitals at 340 and 535 K, and those in Fig. 6(*b*) due to $4f(j = 5/2)\Gamma_7$ orbitals at 430 K, which agree with the directions that the $4f(j = 5/2)$ orbitals specify. 5*d* peaks at 340 and 430 K are due to the partially and fully occupied $5d(j = 5/2)\Gamma_8$ orbitals, while those at 535 K are correlated with the electrons in the fully and partially occupied $5d(j = 5/2)\Gamma_7$ orbitals in refinements (*F*) and (*G*). The relative relationships between the energy levels of the $4f(j = 5/2)\Gamma_8$ and Γ_7 orbitals, which are located inside the 5*d* orbitals, vary according to the populations of the 5*d* orbitals, as discussed in §4.2.1 and in our previous paper (MTOT). However, in spite of the occupation of $5d(j = 5/2)\Gamma_8$ orbitals, the energy levels of the $4f(j = 5/2)\Gamma_8$ at 340 K remain lower than those of Γ_7 orbitals. All positive peaks near Ce in Figs. 6(*b*) and (*c*) extend along the lobes of $4f(j = 5/2)\Gamma_7$ and Γ_8. On the other hand, in Fig. 6(*a*) at 340 K the positive peaks near Ce and the negative peaks in the valleys surrounding them are clearly more spherical than those at the other temperatures. This feature seems to be correlated to the κ parameters of the relevant orbitals. The difference-density distribution was drawn after the refinement of each κ parameter to see which one contributed most to the spherical valley around Ce in Fig. 2(*a*). Then it became evident that these negative peaks were produced by the contraction of the $4f(j = 5/2)\Gamma_8$ orbitals and the expansion of the $5p(j = 3/2)$ orbitals with $\kappa = 1.44$ (5) and 0.90 (3) at 340 K. Since κ of $5p(j = 3/2)$ orbitals at three temperatures are equal within error, the spherical valley at 340 K seems to be correlated to the more contracted $4f(j = 5/2)\Gamma_8$ orbitals with a larger κ value. The significantly deeper and more spherical valley in Fig. 6(*a*) seems to indicate that the electron repulsion between the 4*f* and 5*d* orbitals became weaker. In addition to the partially occupied $5d(j = 5/2)\Gamma_8$ orbitals, this effect keeps the energy levels of $4f(j = 5/2)\Gamma_8$ orbitals lower than that of the Γ_7 orbitals at 340 K.

When the residual densities of Ce at the three temperatures are compared, positive peaks on Ce remained high only at 340 K, as described in §4.2. Introduction of molecular orbitals for the B_6 molecules would be necessary to improve the scale factor and accordingly the residual densities. The positive peak may also indicate that the electron configuration or AHV parameters are insufficient to explain the EDD, or that the scattering factors are not good enough, as pointed out by Claiser *et al.* (2004). There seems to be room for improvement in the analysis of EDD of rare-earth compounds.

5.2. Electron population of $4f(j = 5/2)\Gamma_7$ and AHV parameters

The electron population on $4f(j = 5/2)\Gamma_7$ was refined to be zero at 340 and 535 K. In the present study the AHV parameters, electron-population and κ parameters were refined simultaneously. However, when the AHV parameters were refined first and were not refined again after that, as was done at 430 K(MTOT), the $4f(j = 5/2)\Gamma_7$ orbitals were also occupied by a significant number of electrons, 0.26 (7) and 0.21 (10), and the populations of the $4f(j = 5/2)\Gamma_8$ orbitals are 0.38 (4) and 0.38 (10) at 340 and 535 K. Since the simultaneous refinement of the population parameters and those of AHV has a tendency to increase the population of $4f(j = 5/2)\Gamma_8$, it is clear that the AHV model explained too much, but not all of the aspherical characteristics of the EDD. This is different from the results reported on the Gram–Charlier expansion method

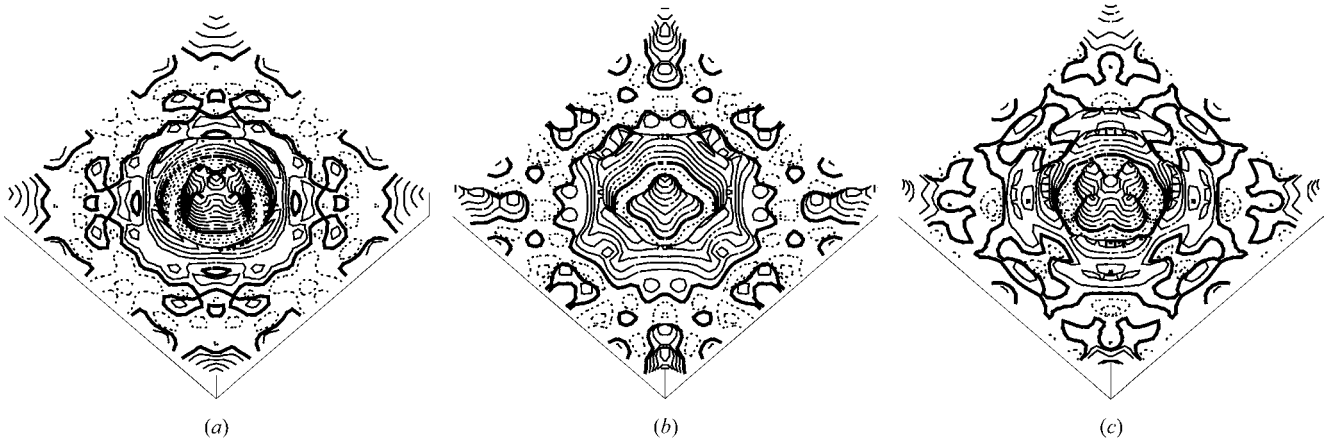

Figure 6
Birds-eye view of deformation densities around Ce after spherical refinement at (*a*) 340, (*b*) 430 and (*c*) 535 K. Contours are as in Fig. 2.

(Mallinson *et al.*, 1988). It became clear that our method of AHV analysis (Dawson *et al.*, 1967; Willis, 1969; Tanaka & Marumo, 1983) does not explain every aspherical EDD. However, the separation of the two aspherical features in EDD owing to electron configuration itself and the aspherical thermal vibrations of atoms is dependent on the number and the accuracy of the higher-order reflections, but it is still a problem to be solved although in the present study lots of time and effort were spent trying to reduce the statistical counting errors for the higher-order reflections.

Positive and negative AHV parameters indicate inhibited and preferential vibrations along the directions that each parameter specifies. q_{1111}, q_{3333}, q_{1122} and q_{1133} express the AHV potential in equation (1) along the ⟨100⟩, ⟨001⟩, ⟨110⟩ and ⟨101⟩ directions. q_{1111} and q_{1122} of Ce in Table 4 were smaller than or insignificant (at all temperatures) compared with those at 298 K (Tanaka & Ōnuki, 2002), where no 5*d* occupation occurs. They were $6\,(2) \times 10^{-12}$ and $-13\,(5) \times 10^{-12}$ erg Å^{-4}, at 298 K. This seems to indicate that the crystal field is made completely different by the electron transfer from the B_6 moiety to Ce. The populations of the B $2p_x$ (= p_y) and $2p_z$ orbitals at 298 K are 0.67 (4) and 0.19 (8), and the κ parameter shows the expansion of B $2p_x$ (= p_y) orbitals making the crystal field of Ce stronger. This tendency of the occupation of the 2*p* orbitals at 298 K is opposite those at 340, 430 and 535 K. The decrease of B $2p_x$ (= p_y) electrons at high temperatures seems to make q_{1111} of Ce insignificant at 430 and 535 K. On the other hand, the increase of the B $2p_z$ orbital at 340, 430 and 535 K suppresses the vibration along ⟨110⟩, where the centre of the B—B_{out} bond is located making q_{1122} positive. The largest q_{1122} value at 430 K may be due to the repulsion between electrons in well localized Ce $4f(j = 5/2)\Gamma_7$ and B $2p_z$ orbitals.

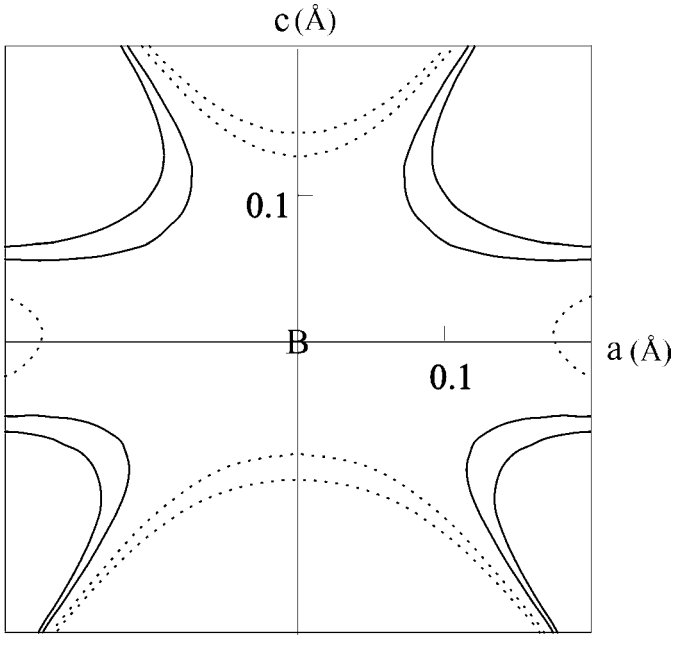

Figure 7
Potential on the 100 plane of anharmonic vibration around B at the centre at 430 K. Contours are at intervals of 1×10^{-23} J. Only the potentials of those absolute values which are smaller than $(1/3)k_BT$(= 2×10^{-23} J) are drawn. Potential at the origin is 0 J. Positive contours are drawn as thin lines, negative contours are drawn as broken lines.

On the other hand, all the quartic AHV parameters of B at 430 K are evidently enhanced compared with those at 340 and 535 K, and all of them except q_{1133} are negative. This may be ascribed to the electrostatic attractive force between the B atom with positive charge and the negative Ce atoms, since the net charge on the Ce atom increases with temperature, *i.e.* −0.88 e at 340 K, −1.62 e at 430 K and −2.84 (refinement *F*) or −2.78 e (refinement *G*) at 535 K. The difference between those at 340 and 430 K may be mainly ascribed to that of the charges. More populated $5d(j = 5/2)\Gamma_8$ orbitals at 430 K extending along ⟨100⟩ may also contribute. However, that between 430 and 535 K may be ascribed to the change of direction of the dominantly occupied 5*d* orbitals, *i.e.* from ⟨100⟩ of $5d(j = 5/2)\Gamma_8$ to ⟨110⟩ of $5d(j = 5/2)\Gamma_7$. In fact, q_{1122} becomes significantly positive at 535 K since the $5d(j = 5/2)\Gamma_7$ orbitals are now fully or partially occupied and suppressed the vibration of B along the ⟨110⟩ direction, although the net charges of B and Ce increased. When Figs. 6(*b*) and (*c*) are compared, it is evident that the distance between the negative charges of B $2p_z$ and Ce $5d(j = 5/2)\Gamma_7$ become closer by the vibration along the ⟨110⟩ directions. At 430 K q_{3333} exhibits strong AHV correlated to the stretching vibration along the B—B_{out} covalent bond, whereas the harmonic temperature factor U^{33} is almost half U^{11} indicating that the harmonic vibration along the bond is suppressed. This may be a result of the interactions among the positive B atom, B $2p_z$ orbitals composing the B—B_{out} bond and the four $5d(j = 5/2)\Gamma_7$ or $5d(j = 5/2)\Gamma_8$ orbitals surrounding it. No electrons in the nearest $5d(j = 5/2)\Gamma_7$ orbitals at 430 K give more freedom to the B atom. While the fully occupied four $5d(j = 5/2)\Gamma_8$ orbitals around the bond on the fourfold axis may possibly enhance the vibration only along the bond, the attractive forces between B and the electrons in the four $5d(j = 5/2)\Gamma_8$ are cancelled except those along the bond when they are combined together. Fully occupied $5d(j = 5/2)\Gamma_7$ orbitals on the other hand attract the B atom in a similar way to that of four fully occupied $5d(j = 5/2)\Gamma_8$ orbitals, but the repulsion between the $2p_z$ orbital and $5d(j = 5/2)\Gamma_7$ orbitals is more severe. In Fig. 7 the anharmonic potential V_A in equation (1) of B at 430 K is drawn on the ⟨100⟩ plane in a square with an edge of 0.4 Å up to $|V_A| < (1/3)k_BT$ (= 2×10^{-23} J). It shows that the vibrations along the ⟨101⟩ directions which q_{1133} specifies seem to be strongly inhibited since it makes the B—B_{out} bond weaker because of the disturbance to the maximum overlap of the $2p_z$ orbitals. Since q_{1133} increased from 65.0×10^{-19} J Å^{-4} at 340 K to 246.1×10^{-19} J Å^{-4} at 430 K, and the population on the $5d(j = 5/2)\Gamma_8$ orbital increased from 0.69 to 1.0, electrostatic repulsion between the electrons in B $2p_z$ and 5*d* orbitals may also be one of the reasons for the increase in q_{1133}.

The discussion here is rather qualitative since the relative effect of each force between charged particles and the stabilization by the B—B_{out} bond is not clear. However, it is evident that significant AHV is observed accompanying the

Table 5
The results of Prince's test among various models at 340, 430 and 535 K.

Prince's test shows that the hypotheses from the two models give equally good fits to the data and can be rejected at $\alpha \times 100\%$ confidence levels. The positive confidence interval λ favours model 1 and the negative interval favours model 2. When $\alpha = 0.5$, this test does not conclude which model is better. At 340 K all independent reflections except {001} were used.

Temperature (K)	Model 1	Model 2	Confidence level α	$(1-\alpha) \times 100\%$ confidence interval λ	Favour model
340	(*B*)	(*C*)	0.005	−0.11142 ± 0.10175	(*C*)
	(*B*)	(*D*)	0.025	−0.11488 ± 0.10829	(*D*)
	(*C*)	(*D*)	0.10	0.09475 ± 0.08680	(*C*)
430	(*B*)	(*C*)	0.005	−0.05528 ± 0.04836	(*C*)
	(*B*)	(*D*)	0.025	−0.04617 ± 0.04090	(*D*)
	(*C*)	(*D*)	0.05	0.09338 ± 0.09099	(*C*)
535	(*B*)	(*C*)	0.0005	−0.06356 ± 0.05782	(*C*)
	(*B*)	(*D*)	0.0005	−0.07746 ± 0.06074	(*D*)
	(*B*)	(*E*)	0.005	−0.08121 ± 0.07563	(*E*)
	(*B*)	(*F*)	0.0005	−0.04767 ± 0.04764	(*F*)
	(*B*)	(*G*)	0.001	−0.04786 ± 0.04587	(*G*)
	(*C*)	(*D*)	0.5	−0.02390 ± 0.02505	–
	(*C*)	(*E*)	0.1	0.03300 ± 0.02851	(*C*)
	(*C*)	(*F*)	0.5	−0.01179 ± 0.01500	–
	(*C*)	(*G*)	0.5	−0.00736 ± 0.01446	–
	(*D*)	(*E*)	0.001	0.08928 ± 0.08687	(*D*)
	(*D*)	(*F*)	0.5	−0.00872 ± 0.02514	–
	(*D*)	(*G*)	0.5	0.00212 ± 0.02581	–
	(*E*)	(*F*)	0.01	−0.05679 ± 0.05300	(*F*)
	(*E*)	(*G*)	0.01	−0.06121 ± 0.05678	(*G*)
	(*F*)	(*G*)	0.1	0.35200 ± 0.35041	(*F*)

change in the electron configuration and the AHV parameters obtained seem to be consistent with a change in the orbital parameters with temperature. The positive q_{1122} at 535 K supports refinements (*F*) and (*G*) at 535 K. We cannot determine which fits best, but we can at least point out that the repulsive interaction between B $2p_z$ and $5d(j = 5/2)\Gamma_7$ electrons is larger in model (*F*).

5.3. Bond lengths and population of $5d(j = 5/2)\Gamma_7$ and $4f(j = 5/2)\Gamma_7$

In our previous study on CeB_6 at 298 K (Tanaka & Ōnuki, 2002) it was assumed that the $B-B_{out}$ bond became shorter to avoid the repulsion between the 4*f* electrons of Ce and 2*p* electrons of B when the $4f(j = 5/2)\Gamma_7$ orbital was occupied. The population was 0.042 (36) at 298 K. The repulsion between $5d(j = 5/2)\Gamma_7$ and 2*p* electrons of B is expected to have a similar effect. Therefore, the $B-B_{out}$ bond lengths and the Γ_7 population of $5d(j = 5/2)$ at 535 K or $4f(j = 5/2)$ at the other temperatures from 100 to 535 K are shown in Fig. 8. If the assumption is correct, $4f(j = 5/2)\Gamma_7$ is also occupied at 340 K. The residual density at 340 K in Fig. 3(*b*) after refinement (*C*) has a peak on Ce extending in the ⟨110⟩ directions. No population of $4f(j = 5/2)\Gamma_7$ orbitals is obtained at 340 K, but when the AHV parameters were refined before the XAO analysis and were fixed in the following refinement, the population of $4f(j = 5/2)\Gamma_7$ orbitals converged to 0.26 (7), but with a higher *R* factor of 0.777% than that of refinement (*C*). Since the bond lengths at 298 and 340 K are equal, and from the facts just stated, there may be $4f(j = 5/2)\Gamma_7$ electrons. When the Γ_7 population increased at 430 K to 0.61 (23) in $4f(j = 5/2)$ orbitals, $B-B_{out}$ became shorter. Then the Γ_7 population decreased to 0.41 (7) in $5d(j = 5/2)$ orbitals and after refinement (*G*) at 535 K it becomes a little longer. If the results of refinement (*F*) with the fully occupied $5d(j = 5/2)\Gamma_7$ orbital is accepted, the $B-B_{out}$ bond should become shorter. Judging by the bond lengths of the $B-B_{out}$ bond that seem to be more reliable than the population and AHV parameters, refinement (*G*) is better than refinement (*F*). However, since the interaction between AHV and orbital parameters are not fully solved, we cannot determine definitely which model is better in the present study.

5.4. Residual peaks

After refinement (*C*) in Table 2 and refinement (*F*) or (*G*) in Table 3 significant peaks still exist on the residual density in Fig. 3(*b*) and Fig. 5(*c*). Since the XAO analysis does not have two-centre scattering models, naturally the largest peaks remain on the $B-B_{out}$ bonds, which are due to the two-centre electrons of the covalent B—B bond. The residual peaks in the 5*d* area are still significant with peak heights more than 0.33 e Å^{-3}. Since peaks of 5*d* electrons at the 5*d* area can produce very small peaks with heights of at most 0.22 e Å^{-3}, as shown in Fig. 4, the residual peaks are too large to express even with the fully occupied 5*d* orbital, as seen in the difference between the relevant peaks in Figs. 5(*b*), (*c*) and (*d*). The CeB_6 crystal is very hard and the reflections with 2θ greater than 150° are still significant so the series termination effect cannot be dismissed, as pointed out by Tanaka & Ōnuki (2002). In fact, the peaks in the 5*d* area surround the Ce

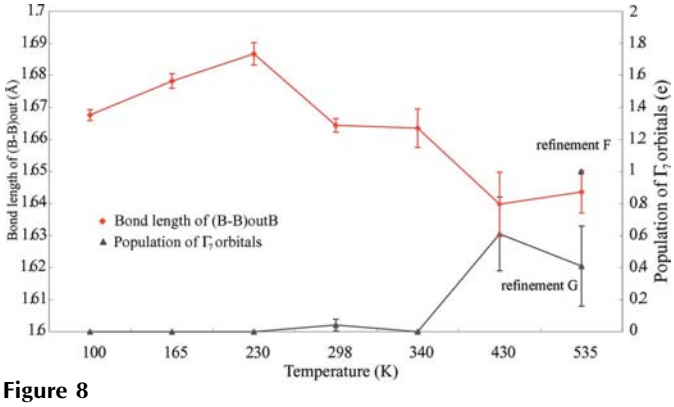

Figure 8
The bond lengths of $B-B_{out}$ and the population of Γ_7 orbitals at temperatures from 100 to 535 K. The bond length and population at 100, 165, 230, 298 K were quoted from Tanaka & Ōnuki (2002). The populations at 298 and 430 K are $4f(j = 5/2)\Gamma_7$ orbitals and those at 535 K are $5d(j = 5/2)\Gamma_7$ orbitals.

atom spherically. Thus, the orbital parameters obtained in the present study may possibly be improved when reliable intensity measurement is carried out with synchrotron radiation using a short wavelength by avoiding the multiple diffraction effect. When many reliable intensities of high-order reflections are collected, the separation of the two aspherical EDD due to electron configuration and AHV is also improved.

5.5. Reduction of *R* factors and its significance

Since the *R* factor after the spherical atom refinement (refinement *A*) is $\sim 1\%$, room for the reduction of *R* factors is very small and the *R* factors after XAO analysis reduced only a little. Hamilton's significance test (Hamilton, 1965) and Prince's test (Prince, 1982) were carried out to judge the validity of the refinements. The R_1(refinement *B*)/R_1(refine-(refinement *C*) ratio at 340 K and R_1(refinement *B*)/R_1(refinement *F*) ratio at 535 K are 1.024 and 1.071. These satisfied the significant levels $\alpha = 0.05$ ($R_{2,154,0.05} = 1.020$) and $\alpha = 0.005$ ($R_{3,145,0.005} = 1.045$). Hamilton's significance test shows at least that the refinement including 5*d* orbitals is more valid than that without 5*d* orbitals. Table 5 shows the result of Prince's test using the independent reflections at 340, 430 and 535 K that can compare two models with the same number of parameters. Prince's test shows that the hypothesis that two models give equally good fits to the data can be rejected at $\alpha \times 100\%$ confidence levels. Prince's test shows that the refinements with 5*d* orbitals are much better than refinement (*B*), except at 340 K. When all independent reflections are used at 340 K, the confidence level α between refinements (*B*) and (*C*), (*B*) and (*D*), (*C*) and (*D*) is 0.5, 0.25 and 0.025. This discrepancy is led by the {001} reflection used in refinements (*C*) and (*D*). {001} reflections have only two equivalents, 001 and 100. $F_o(001)$ is smaller than $F_o(100)$ and $|F_o(001) - F_c(001)|$ is large, which may be caused by the Pt wire of the furnace. Hence, results at 340 K without the {001} reflection are listed in Table 5. At 430 K, Prince's test shows that refinement (*C*) is better than (*B*) and (*D*). On the other hand, although Prince's test at 535 K can conclude that refinements (*B*) and (*E*) are less valid than others, there are no significant differences among refinements (*C*), (*D*), (*F*) and (*G*) except the difference between (*F*) and (*G*). If the confidence level $\alpha = 0.1$ is significant for XAO analysis, refinement (*F*) may be better than refinement (*G*).

Since the directions that 4*f* and 5*d* orbitals, and AHV parameters specify are known, we can judge if the parameters obtained in XAO correspond well to the peaks of the difference density after refinement (*A*) in Fig. 6, which exhibits the observed aspherical EDD. Let us note that the 0.142 and 0.128% reduction of R_1 and R_2 factors from refinements (*A*) to (*B*) at 340 K in Table 2 accompany the reduction of the $4f(j = 5/2)\Gamma_8$ peak on Ce in Fig. 1(*a*) from 0.8 to -0.06 e Å^{-3}. This indicates that the 0.1% reduction in *R* factors is valid in the present study. As has already been discussed, it is evident that the 0.018 and 0.024 reduction of R_1 and R_2 from refinement (*B*) to (*C*) is due to the occupied $5d(j = 5/2)\Gamma_8$ orbitals. It reduces the 5*d* peak height $\Delta\rho_A$ in Table 2 from 0.56 to 0.37 e Å^{-3}. Accordingly, the 0.02% reduction of *R* factors may be taken as significant improvement. However, the *R* factors of refinements (*C*) and (*D*) are almost equal and it is not possible to discriminate between (*C*) and (*D*). $\Delta\rho_A$, 0.45 e Å^{-3}, of refinement (*D*) which is due to the occupied $5d(j = 3/2)\Gamma_8$ orbital is 0.08 e Å^{-3} higher than (*C*). As stated in §4.2.1, $5d(j = 5/2)\Gamma_8$ extends along ⟨100⟩, while $5d(j = 3/2)$ has spherical EDD, which resulted in a difference of 0.08 e Å^{-3} for $\Delta\rho_A$. AO and AHV behave properly to fit to the experimental difference density in the XAO analysis.

Table 6
Electrons of the 5*d*-peak in the unit cell remaining after each refinement in the residual density map at 340, 430 and 535 K.

Temperature (K)	340	430	535
(*B*)	1.56	2.45	1.05
(*C*)	0.89	1.57	0.70
(*D*)	0.92	1.46	0.66
(*E*)	–	–	0.82
(*F*)	–	–	0.51
(*G*)	–	–	0.52

The orbital parameters express the local EDD around the atom and thus the *R* factors which take all the diffraction effects into account may not be a good measure. There was no clear measure to judge the validity of the refinement for such a system with highly condensed electrons. Replacing $||F_o| - |F_c||$ in R_1 and R_2 by σF_o, a statistical counting error of F_o, $S_1 = \Sigma||\sigma F_o|/\Sigma|F_o|$ and $S_2 = \{\Sigma(\sigma F_o)^2/\Sigma|F_o|^2\}^{1/2}$ are calculated to estimate the *R* values when the aspherical EDD was refined well and systematic errors were corrected well. The differences between the *R* factors after the spherical atom refinement (*A*) and S_i values express the room left for the XAO analysis. $D_1 = R_1$(refinement *A*) $- S_1$ and $D_2 = R_2$(Refinement *A*) $- S_2$ are 0.497 and 0.783%, at 340 K, and 0.610 and 0.680% at 535 K. Refinements (*B*) explain 29% of D_1 and 16% of D_2 at 340 K, and 16% of D_1 and 18% of D_2 at 535 K. Further refinements including 5*d* orbitals increase these numbers to 32 and 19% at 340 K, 26% of D_1 and 33% of D_2 in refinement (*F*) at 535 K.

In order to see how much 5*d* electrons are taken into account let us integrate directly the 5*d* area on the residual density map after refinements (*B*) and refinements with 5*d* orbitals. The number of residual electrons after the refinements at 340, 430 and 535 K are listed in Table 6. The difference in the numbers of residual electrons between refinements (*B*) and (*C*) at 340 and 430 K, and between refinements (*B*) and (*F*) at 535 K are 0.67, 0.88 and 0.54. Although the heights of the 5*d* peaks are low, the numbers of electrons explained by the refinements of 5*d* orbitals seem to be significant.

6. Conclusion

According to the XAO analysis electrons are transferred from the B $2p_x$ ($= p_y$) orbitals to the Ce 4*f* and 5*d* orbitals at 340, 430 and 535 K. Since highly localized 4*f*-EDD was clearly explained, we can conclude first that 4*f*-EDD can be observed and analyzed with the orbital models based on quantum

mechanics. The 5*d* occupation is commonly observed in the present work and in MTOT at 430 K. Therefore, our second conclusion in our series of investigations is that the B 2*p* electrons are transferred to Ce 5*d* orbitals and the 5*d*-EDD can also be analyzed based on a quantum-mechanical AO model. The third conclusion is that the $4f(j = 5/2)\Gamma_8$ orbitals are more populated than $4f(j = 5/2)\Gamma_7$ orbitals at 340 and 535 K, which is different from our previous study at 430 K, but agrees with that at 298 K (Tanaka & Ōnuki, 2002). The electron transfer between B and Ce changes the order of the energy levels of the 4*f* orbitals located inside the 5*d* orbitals that accept most of the transferred electrons. The AHV analysis at the three temperatures also supports the different electron configuration at the three temperatures.

Since the accuracy of the measurement of the present study is very close to the experimental error, as is seen in the slight improvement of *R* factors which was discussed in MTOT, more accurate measurement is desirable for future EDD investigations, especially of heavy-atom crystals. The separation of the aspherical distribution of EDD due to the electron configuration and the vibrations of atoms seems to remain as an unsolved problem. The series termination effect of the Fourier summation makes the EDD of 5*d* orbitals, which exhibits diffuse peaks at the 5*d*-area, less reliable. Accurate intensity measurement of high-order reflections avoiding the multiple diffraction effect by using synchrotron radiation with a short wavelength is very important to solve these problems. The recent development of neutron diffraction is also expected to give reliable temperature factors of nuclei and the combined use with X-rays seems to have high potential to solve the problem.

The present study reveals a fruitful future for the rare-earth complexes as a quantum material, since electrons are transferred below 473 K to the 5*d* state with an energy of *ca* 4×10^4 to 7×10^4 K (program *HEX* by Liberman *et al.*, 1971; Martin *et al.*, 1978) above the 4*f* states which are not fully occupied, forming the state of population inversion. If the 5*d* $\rightarrow$ 4*f* transition can be made by *e.g.* a UV stimulated transition, the emitted light can be a very useful energy source utilizing the low-quality discarded heat below 473 K.

References

Becker, P. J. & Coppens, P. (1974*a*). *Acta Cryst.* A**30**, 129–147.
Becker, P. J. & Coppens, P. (1974*b*). *Acta Cryst.* A**30**, 148–153.
Becker, P. J. & Coppens, P. (1975). *Acta Cryst.* A**31**, 417–425.
Claiser, N., Souhassou, M. & LeComte, C. (2004). *J. Phys. Chem. Solids*, **65**, 1927–1933.
Dawson, B., Hurley, A. C. & Maslen, V. W. (1967). *Proc. R. Soc. London Ser. A*, **298**, 289–306.
Dyall, K. D., Grant, I. P., Johnson, C. T., Parpia, F. A. & Plummer, E. P. (1989). *Comput. Phys. Commun.* **55**, 425–456.
Grushko, Yu. S., Paderno, Yu. B., Mishin, K. Ya., Molkanov, L. I., Shadrina, G. A., Konovalova, E. S. & Dudnik, E. M. (1985). *Phys. Status Solidus B*, **128**, 591–597.
Hamilton, W. C. (1965). *Acta Cryst.* **18**, 502–510.
Heide, P. V. D., Cate, H. W. T., Dam, L. M. T., Groot, R. A. D. & Vroomen, A. R. D. (1986). *J. Phys. Metal Phys.* **16**, 1617–1623.
Ignatov, M. I., Bogach, A. V., Demishev, S. V., Glushkov, V. V., Levchenko, A. V., Paderno, Yu. B., Shitsevalova, N. Yu. & Sluchanko, N. E. (2006). *J. Solid State Chem.* **179**, 2805–2808.
Kamimura, H., Sugano, S. & Tanabe, Y. (1969). *Ligand Field Theory and its Application.* Tokyo: Syōkabō (in Japanese).
Liberman, D. A., Cormer, D. T. & Waber, J. T. (1971). *Comput. Phys. Commun.* **2**, 107–113.
Loewenhaupt, M., Carpenter, J. M. & Loong, C.-K. (1985). *J. Magn. Magn. Mater.* **52**, 245–249.
Makita, R., Tanaka, K., Ōnuki, Y. & Tatewaki, H. (2007). *Acta Cryst.* B**63**, 683–692.
Mallinson, P. R., Koritsanszky, T., Elkaim, E., Li, N. & Coppens, P. (1988). *Acta Cryst.* A**44**, 336–343.
Mann, J. B. (1968). Report LA3691. Los Alamos National Laboratory, New Mexico, USA.
Martin, W. C., Zalubas, R. & Hagan, L. (1978). *Atomic Energy Levels – The Rare Earth Elements.* NSRDS-Natl, Washington: National Bureau of Standards, US Department of Commerce.
Nagao, T. & Igarashi, J. (2002). *J. Phys. Soc. Jpn*, **71**, 1771–1779.
Okada, K., Kaizu, Y., Kobayashi, H., Tanaka, K. & Marumo, F. (1985). *Mol. Phys.* **54**, 1293–1306.
Prince, E. (1982). *Acta Cryst.* B**38**, 1099–1100.
Sakai, O., Shiina, R., Shiba, H. & Thalmeier, P. (1997). *J. Phys. Soc. Jpn*, **66**, 3005–3007.
Sakurai, T. & Kobayashi, K. (1979). *Rep. Inst. Phys. Chem. Res.* **55**, 69–77.
Sato, N., Sumiyama, A., Kunii, S., Nagano, H. & Kasuya, T. (1985). *J. Phys. Soc. Jpn*, **54**, 1923–1932.
Souma, S., Iida, Y., Sato, T., Takahashi, T. & Kunii, S. (2004). *Physica B*, **351**, 283–285.
Streltsov, V. A., Konovalova, E. S. & Paderno, Yu. B. (1999). *Physica B*, **259–261**, 1155–1156.
Tanaka, K., Kumazawa, S., Tsubokawa, M., Maruno, S. & Shirotani, I. (1994). *Acta Cryst.* A**50**, 246–252.
Tanaka, K., Makita, R., Funahashi, S., Komori, T. & Zaw Win (2008). *Acta Cryst.* A**64**, 437–449.
Tanaka, K. & Marumo, F. (1983). *Acta Cryst.* A**39**, 631–641.
Tanaka, K. & Ōnuki, Y. (2002). *Acta Cryst.* B**58**, 423–436.
Thornley, F. R. & Nelmes, R. J. (1974). *Acta Cryst.* A**30**, 748–757.
Willis, B. T. M. (1969). *Acta Cryst.* A**25**, 277–300.
Zirngiebl, E., Hillerbrands, B., Blumenroder, S., Guntherodt, G., Loewenhaupt, M., Carpenter, J. M., Winzer, K. & Fisk, Z. (1984). *Phys. Rev. B*, **30**, 4052–4054.